HHS Public Access

Author manuscript

Dev Biol. Author manuscript; available in PMC 2024 February 01.

Published in final edited form as:

Dev Biol. 2023 February ; 494: 71–84. doi:10.1016/j.ydbio.2022.12.003.

Tbx2 and *Tbx3* regulate cell fate progression of the otic vesicle for inner ear development

Hansoo Song,

Bernice Morrow

Department of Genetics, Albert Einstein College of Medicine, 1301 Morris Park Ave., Bronx, New York 10461, USA

Abstract

The morphogenesis of the otic vesicle (OV) to form inner ear organs serves as an excellent model system to understand cell fate acquisition on a single cell level. *Tbx2* and *Tbx3* (*Tbx2/3*) encode closely related T-box transcription factors that are expressed widely in the mammalian OV. Inactivation of both genes in the OV (*Tbx2/3*cKO) results in failed morphogenesis into inner ear organs. To understand the basis of these defects, single cell RNA-sequencing (scRNA-seq) was performed on the OV lineage, in controls versus *Tbx2/3*cKO embryos. We identified a multipotent population termed otic progenitors in controls that are marked by expression of the known otic placode markers *Eya1*, *Sox2*, and *Sox3* as well as new markers *Fgf18*, *Cxcl12*, and *Pou3f3*. The otic progenitor population was increased three-fold in *Tbx2/3*cKO embryos, concomitant with dysregulation of genes in these cells as well as reduced progression to more differentiated states of prosensory and nonsensory cells. An ectopic neural population of cells was detected in the posterior OV of *Tbx2/3*cKO embryos but had reduced maturation to delaminated neural cells. As all three cell fates were affected in *Tbx2/3*cKO embryos, we suggest that *Tbx2/3* promotes progression of multipotent otic progenitors to more differentiated cell types in the OV.

Graphical Abstract

Correspondence to Bernice E. Morrow. bernice.morrow@einsteinmed.edu.

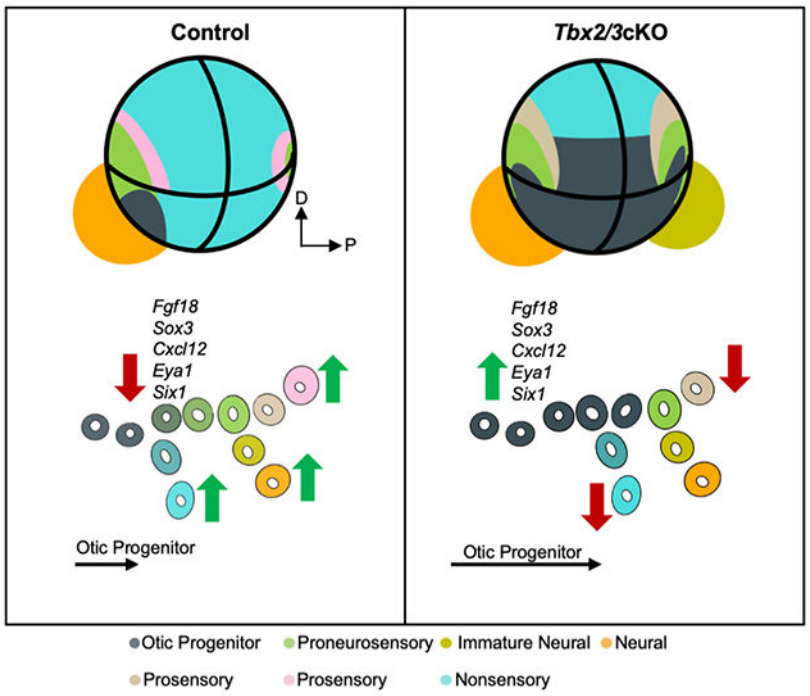

Keywords

Inner Ear; Otic Vesicle; Tbx2; Tbx3; Conditional Knockout; Single-cell RNA-Sequencing; Cell fate

1. Introduction

The mammalian inner ear consists of the auditory and vestibular systems. The auditory system is composed of the organ of Corti, located within the cochlea and is responsible for hearing. The vestibular organs are composed of the semicircular canals (SCCs) and the ampullae with their respective cristae, as well as the utricle and saccule with their respective maculae and are responsible for sensing body movement. There are three main cell types in the inner ear, termed the sensory, nonsensory, and neural (Bok et al., 2007; Morsli et al., 1998). Sensory hair cells and adjacent nonsensory support cells are located in the organ of Corti and crista ampullaris of the vestibular organs. Sound and movement detected by sensory cells are transmitted to the cochlear and vestibular branches of the cochleovestibular nerve, respectively (Torres & Giráldez, 1998).

Each of the inner ear organs undergoes crucial morphological changes during embryonic development and begins with a simple ectodermal thickening lateral to the developing head, termed the otic placode, which invaginates and then pinches off from the ectoderm to form the otic vesicle (OV) (Chatterjee et al., 2010; Morsli et al., 1998). The development of the otic placode into the OV is heavily influenced by anterior-posterior (A-P) and dorsal-ventral (D-V) signaling gradients to guide formation of distinct compartments within the OV to promote region specific gene expression (Bok, Raft, Kong, Koo, Drager, et al., 2011; Lin

et al., 2005; Raft & Groves, 2015; Riccomagno et al., 2002a). The proneurosensory cells in the anteroventral domain of the OV give rise to neural progenitors that delaminate and develop into the cochleovestibular ganglion (CVG) and prosensory cells that develop into sensory hair cells in both anterior and posterior domains of the OV. The proneurosensory cells express marker genes such as *Fgf10* (Pauley et al., 2003), *Gata3* (Duncan & Fritzsch, 2013; Lilleväli et al., 2006), *Six1* (Ahmed et al., 2012; Ozaki et al., 2004; Schlosser et al., 2008; Wong et al., 2013; Zhang et al., 2017; Zheng et al., 2003), and *Eya1* (Ahmed et al., 2012; Freyer & Morrow, 2010; Friedman et al., 2005; Wong et al., 2013). These cells have also previously been uncovered by single cell qRT-PCR analysis of OV cells in which additional gene markers, *Sox2* and *Lfng* were identified (Durruthy-Durruthy et al., 2014). The neural progenitor cells prior to and during delamination to form the CVG express the transcription factor genes, *Neurog1* (Hartman et al., 2015; Ma et al., 1998, 2000) and *NeuroD1* (Jahan et al., 2010), while more mature, delaminated CVG cells express *Rgs4* that encodes a protein, which regulates G-protein signaling (Kim et al., 2014). Prosensory cells form hair cells of the cochlea and vestibular organs and are marked by continued expression of the transcription factor gene, *Sox2* (Kiernan et al., 2005) and *Gata3* (Economou et al., 2013; Lilleväli et al., 2006; Luo et al., 2013) as well as prosensory specific expression of signaling genes, *Jag1* (Adam et al., 1998; Cole et al., 2000; Morrison et al., 1999), *Bmp4* (Blauwkamp et al., 2007; H. Li et al., 2005; Ohyama et al., 2010; Wu & Oh, 1996), and *Fgf10* (Pauley et al., 2003), for formation of vestibular organs. The dorsal-ventral axis arises during invagination of the otic placode (Bok et al., 2007; Wu et al., 1998) in which nonsensory homeodomain genes, *Dlx5* and *Otx2* mark the dorsal and ventral domains of the OV, respectively (Morsli et al., 1999; Robledo & Lufkin, 2006). The medial-lateral (M-L) axis forms last and is speculated to form as part of the invagination process of the otic placode to form the otic cup, as seen by medial expression of *Pax2* (Whitfield & Hammond, 2007).

T-box transcription factors have been identified to be crucial for the development of many organs. *Tbx2* and *Tbx3* act as transcriptional repressors and promote cell proliferation, maintain survival, and modulate cell fate during the development of many organs such as in the limb, lung, and heart (Farin et al., 2013; Lüdtke et al., 2016; Mesbah et al., 2012). We therefore decided to further investigate the functions of *Tbx2* and *Tbx3* (*Tbx2/3*), both of which are expressed in the OV (Kaiser et al., 2021; Zirzow et al., 2009). *Tbx2/3* are similar genes formed by a gene duplication event during vertebrate evolution (Papaioannou, 2014). They retain 95% amino acid similarity in the DNA binding domain and 54% similarity overall (National Center for Biotechnology Information-NCBI, BLAST software). They also have overlapping patterns of expression, supporting the observation that *Tbx2/3* have significant shared functions in embryogenesis (Coll et al., 2002; Papaioannou, 2014). Recently, *Tbx2/3* were inactivated in the mouse OV and this severely disrupted inner ear morphogenesis. Through analysis of OV domain gene markers and known genetic pathways important for organizing inner ear morphogenesis in control and mutant embryos, it was suggested that *Tbx2/3* functions to restrict neurogenesis in the otic vesicle (Kaiser et al., 2021). Although this prior investigation implicated *Tbx2/3* functions in restricting neurogenesis, this study did not include transcriptomic analysis on a single cell level (Kaiser et al., 2021). We furthered this work by validating many of the previous phenotypic findings

of the importance of *Tbx2/3* in inner ear development using different *Tbx2/3* floxed mice. These mice were also maintained in a different background, which together may have led to the slight differences in phenotypic findings at early stage. However, the major defects in morphogenesis were consistent with the previous study. By performing single cell RNA-sequencing (scRNA-seq) we provide further insights into the cellular and molecular causes of failed inner ear morphogenesis in mutant OVs.

To further our understanding of *Tbx2/3* functions in early development, we carefully analyzed our *Tbx2* and *Tbx3* double conditional knockout (*Tbx2/3*cKO) mouse model for defects in inner ear morphogenesis in the OV after gene inactivation. We confirmed that there was a severe lack of development from the OV stage and found the earliest morphological defect was an expansion of the A-P axis of the OV in *Tbx2/3*cKO embryos at stage E10.5. We identified slight changes in the position of apoptotic domains of the OV, but did not observe changes in rates of apoptosis or cell proliferation at this stage. We then performed scRNA-seq followed by whole mount *in situ* RNAscope (wmRNAscope) analysis to understand how changes detected by scRNA-seq translated to three-dimensional expression changes in mutant embryos at E10.5. We uncovered a multipotent population that we term otic progenitor cells, localized near the proneurosensory domain of the OV. The relative proportion of this otic progenitor population was greatly expanded in *Tbx2/3*cKO embryos, along with dysregulated gene expression leading to failed differentiation into mature inner ear cell types.

2. Materials & Methods

2.1. Mouse strains

Pax2-Cre (Ohyama & Groves, 2004) and *Pax8-Cre* (Bouchard et al., 2004) transgenic mice and their lineage contributions to the inner ear have previously been described. To generate $Tbx2^{f/f}$ and $Tbx3^{f/f}$ mice, two LoxP sites were inserted into the intronic sequences flanking exon 2 (*Tbx2*) and exons 2-4 (*Tbx3*), respectively, by gene targeting using homologous recombination (Dr. Chenleng Cai, Indiana U.). The reading frame and the T-box domain of *Tbx2/3* were disrupted following recombination. Primer sequences indicate the position of the deleted region (Supplemental File 1). All the mouse lines used in this study were maintained in an outbred SwissWebster genetic background. $Tbx2^{f/f};Tbx3^{f/f}$ mice were intercrossed for over 10 generations. $Tbx2^{f/f};Tbx3^{f/f}$ mice were crossed with $Rosa26\text{-}GFP^{f/f}$ (RCE:loxP) mice (Sousa et al., 2009) and the $Tbx2^{f/+};Tbx3^{f/+};Rosa26\text{-}GFP^{f/+}$ mice were intercrossed to generate $Tbx2^{f/f};Tbx3^{f/f};Rosa26\text{-}GFP^{f/f}$ mice. Primers used for genotyping embryos and mice are provided in the Supplemental File 1. Mouse embryos were collected in phosphate-buffered saline (PBS). Yolk sac or hind limbs were collected from each embryo and used for genotyping. Mouse embryos were staged based on somite counts and vaginal plug dates (E0.5). Somite counts for stage E8.5 was 8-11 somite pairs, E9.0 was 18-21 somite pairs, E9.5 was 24-27 somite pairs and E10.5 was 34-37 somite pairs. E13.5 and E15.5 stages were determined based on vaginal plug dates. Female and male embryos were used indiscriminately for all experiments, and we did not genotype embryos for sex. Both left and right OV's and inner ears were used for all experiments. All mouse studies were conducted according to protocols approved by the Institutional Animal Care of

Use Committee at Albert Einstein College of Medicine (#00001034; https://einsteinmed.org/administration/animal-care-use-committee/).

2.2. Paint filling

Embryos for paint filling at E13.3 and E15.5 were fixed in Bodian's fixative overnight (O/N) at room temperature (RT). Embryos were washed with and placed in 100% ethanol O/N at RT. Embryos were cleared in methyl salicylate O/N at RT. Embryo heads were cut in half to separate the left and right sides. The brain and brainstem of embryos were carefully removed. A 0.2% solution of BiC White-Out in methyl salicylate was used to microinject inner ears. The inner ear labyrinths in cleared heads were visualized using a Leica MZ125 stereo microscope.

2.3. H&E histology

Embryos were collected at E13.5 and E15.5 and fixed in 10% formalin O/N. After fixation, embryos were processed through two washes of PBS for 10' ('; min) each followed by a 1 hr (hr; hour) incubation in xylene. The xylene wash was repeated with fresh xylene for 1hr. Embryos were then placed in Tissue Prep 2 Paraffin (Fisher Scientific, T555) at 65°C for 1hr with one additional exchange of paraffin. Embryos were oriented in paraffin and sectioned at 12μm (μm, microns). Sections were incubated at 39°C O/N. Sections were cleared using xylene, stained with hematoxylin and eosin (H&E), and mounted using Permount. Stained sections were visualized using a Zeiss Axioskop 2 Plus microscope.

2.4. OV measurements

The OV measurements of control and *Tbx2/3*cKO embryos were performed by imaging whole embryos directly after dissections with a Zeiss Stereo Discovery microscope. FIJI ImageJ software was used to measure the A-P and D-V axis. The M-L and D-V axes were measured using FIJI ImageJ software after immunofluorescence and TUNEL assays. Measurements of D-V axes before and after sectioning were used to confirm consistency.

2.5. Immunofluorescence and TUNEL assays

For immunofluorescence, embryos were dissected at E10.5 or E11.5 and fixed in 4% paraformaldehyde in PBS at 4°C (C, Celsius) for 1hr. Embryos were washed in PBS and dehydrated using 70%/90%/100% ethanol. Embryos were washed twice in xylene for 1hr at RT. Xylene was removed and embryos were embedded in paraffin and stored as described for H&E sectioning. Rabbit anti-phospho-Histone H3 antibodies (1:200; Ser10; Millipore, 06-570) was used to mark proliferating cells. Mouse anti-ISL1 antibodies (1:1:98; Developmental Studies Hybridoma Bank, 39.4D5-S & 39.4D5-C) was used to identify the CVG. Donkey anti-rabbit IgG Alexa Fluor 647 (1:200; Invitrogen, A31573) was used as a secondary antibody for anti-PH3 and donkey anti-mouse IgG Alexa Fluor 568 (1:200; Invitrogen, A10037) was used as a secondary antibody for anti-ISL1. For TUNEL experiments, the procedure provided by "*In Situ* Cell Death Detection Kit, TMR red" Kit version 12, Roche March 2016 (Cat. No. 12 156 792 910) was used directly following washes after secondary antibody incubation for immunofluorescence as above. Slides were cover slipped using VectaSheild®HardSet™ with DAPI (Vector Laboratories, H-1500-10)

and stored at 4°C until imaging. Imaging was done using an Apotome Zeiss microscope. Counting of the cells was performed using Fiji ImageJ software.

2.6. wmRNAscope

After dissections, embryos at E8.5-10.5 were fixed O/N in 4% Paraformaldehyde in PBS at 4°C. For storage, embryos were dehydrated using 2 washes of 10' each of a serial dilution of 25/50/75/100% methanol. Embryos were stored in 100% methanol at −20°C. When ready for use, embryos were rehydrated in reverse order of serial dilution of methanol into a final PBS+0.1% Tween solution. Embryos were further dissected to expose the neural tube by cutting the top of the head and cutting just below the forelimb buds. This was done to reduce background staining and signal resulting from trapped probes. After rehydration, embryos were washed twice in PBS+0.1% Tween for 5' each. Embryos were then permeabilized at RT by incubating in Protease III (provided in kit) for 20'. Embryos were then washed 3 times in PBS+0.01% Tween for 5' each. During the permeabilization step, a probe master mix was prepared using C1, C2, and C3 as needed (RNAscope probes; Supplemental File 2). C1, C2, and C3 probes were warmed individually in a hybridization oven for 10' at 40°C and mixed at a 50:1:1 ratio. Embryos were incubated O/N in 100μL (microliters; μL) of probe master mix at 40°C. For all following washes, three washes were performed for 5' each at RT using a 0.2X SSC + 0.01% Tween solution. After hybridization, embryos were washed and then incubated for 10' in 4% paraformaldehyde in PBS at RT. Embryos were incubated in AMP1 (provided in kit) for 30' at 40°C followed by AMP2 for 30' at 40°C and then AMP3 for 15' at 40°C with washes in between each AMP step followed by HRP (hydrogen peroxidase) treatment. TSA (Tyramide Signal Amplification) fluorophores were prepared at 1:2,000, 1:1,000, and 1:500 dilution for TSA-CY3, TSA-CY5, and Fluorescein respectively. Embryos were incubated in HRP-C1 for 15' at 40°C. Washes were done and then embryos were incubated in the selected TSA for the C1 probe for 30' at 40°C. After binding of the TSA to the HRP embryos were incubated in HRP-blocker to prevent future reactions with the other TSA. The previous steps from incubation with HRP to HRP-blocker were repeated per channel used, with washes in between each step. Embryos were then incubated in DAPI for 2 days followed by a final wash and stored at 4°C until ready for imaging. Z-stack images were taken (Analytical Imaging Facility; Albert Einstein College of Medicine) and 3-D reconstructions of Z-stack images were done using Fiji ImageJ software.

2.71. ScRNA-seq—Two replicates of control, *Pax2-Cre;Rosa26-GFP*$^{f/+}$ embryos and two replicates of mutant *Pax2-Cre;Tbx2*$^{f/f}$*;Tbx3*$^{f/f}$*;Rosa26-GFP*$^{f/+}$ embryos were used for scRNA-seq experiments. Three control embryos and two *Tbx2/3*cKO mutant embryos were collected per replicate at E10.5 (34s-36s). Embryos were dissected in PBS with Ca2+ and Mg2+ and placed in ice cold DMEM while embryos were genotyped. After genotyping, embryos were placed back into PBS with Ca^{2+} and Mg^{2+}. Genotyping was optimized using Phire PCR mix (ThermoFisher, Cat# F170S) to allow completion within 1hr. The OV with CVG were microdissected to remove as much surrounding tissue as possible (adjacent neural tube with pharyngeal cells). Microdissected OVs were pooled in DMEM (GIBCO, Cat# 11885-084) at 4°C followed by centrifugation at 100 x g for 5' at 4°C. DMEM was removed, and tissues were incubated with 0.25% Trypsin-EDTA (GIBCO, Cat# 25200-056) containing DNase I (50U/mL) (Millipore, Cat# 260913-10MU) for 10' at RT. FBS (heat

inactivated, ATCC, Cat#30-2021) was added to terminate DNase I activity. Cells were centrifuged at 4°C at 300 x g for 5', supernatant was removed, and cells were resuspended in PBS w/o Ca^{2+} and Mg^{2+} (Corning, Cat# 21-031-cv) with 10% FBS and filtered through a 100μm cell strainer. DAPI (Thermo Fisher Scientific, Cat# D3571) was added before cell sorting was performed to remove the lysed cells. After filtering, the cells were sorted with the BD FACS Aria II system (Flow Cytometry Core Facility, Albert Einstein College of Medicine). The sorted GFP positive cells were centrifuged in 4°C at 300 x g for 5' and resuspended in 50 μL PBS w/o Ca^{2+} and Mg^{2+} with 10% FBS. Cells were loaded onto a 10x Chromium instrument (10x Chromium Next GEM Single Cell 3' GEM, Dual Index Library & Gel Bead Kit v3.1; 10x Genomics, Cat# PN-1000121) according to manufacturer's specifications. The total number of cells used for each replicate is represented in Fig. S5. The maximum number of cells obtained for the *Tbx2/3*cKO genotype were used as a target for controls, around 4,800 cells. A Qubit®2.0 fluorometer (Thermo Fisher Scientific, Waltham, MA) was used to determine the concentration of the resulting cDNA libraries. A total of 25uL of cDNA library (25 nMolar; average of 195ng per sample) was used for sequencing using the Illumina HiSeq4000 system (Genewiz, South Plainfield, NJ) with paired end, 150bp read length. Each sample was sequenced on a separate flowcell to maximize reads per sample. A total of 9,415 cells were sequenced with a mean read total of 48,100 per cell and 3,687 median genes were obtained per cell. Data generated is available on NCBI Gene Expression Omnibus, GSE185172.

2.72. Computational analysis of scRNAseq data—After the FASTQ files were obtained, the quality of the data was checked using FastQC v0.11.4. After FastQC analysis, sequencing reads were aligned to the mouse reference genome (mm10-2020-A) by Cell Ranger v3.1.0 (10xGenomics). Seurat v 4.1.0 was used to filter and normalize cells using parameters suggested by Seurat software. PCA and UMAPs were generated for each dataset separately. Gene markers for the OV and CVG were used to identify and isolate individual clusters and subclusters.

Velocyto v0.17.17 software was used to generate loom files. The loom files and UMAP information from Seurat were passed to scVelo v0.2.3 to identify cell fates based on RNA velocities from a dynamical model. CellRank v1.5.1 was used to generate directed single-cell fate maps, calculate absorption probabilities, and identify lineage genes. Anndata v0.7.5 was used to calculate velocities. Velocities and expression data were visualized using Matplotlib v3.3.4 and Scanpy v1.7.1.

Seurat objects were passed into RISC v1.0 software to integrate the four samples, two control and two *Tbx2/3*cKO datasets. Control 1 was used as reference for integration as it had the highest number of clusters through a range of principle components tested, which was 11 to 20 PCs. A UMAP was generated using this integrated data to identify differentially expressed genes (DEGs) amongst clusters and known markers of the OV and CVG. Further, DEGs between control and *Tbx2/3*cKO embryos were identified using RISC software, fold change > 0.5 or < −0.5 and adjusted P-value < 0.05. Since the original Seurat cluster identity was retained throughout the datasets processed through Seurat, scVelo, CellRank, and RISC analyses, this information was used to identify where cells were localized within initial state and terminal state clusters within the RISC UMAPs. Two

proportion Z statistical tests were performed to determine significance of cluster and cell type proportions.

2.8. Quantitative PCR (qPCR) assays

Cells were isolated and purified from whole embryos with the same procedure used in scRNA-seq. After flow cytometry cell sorting, cells were centrifuged at 4°C, 300xg, for 5'. Supernatants were removed and 700μL of TRIzol (ThermoFisher, Cat# 15596026) was added. Samples were pipetted up and down multiple times and incubated for 5'. A total of 140μL of Chloroform was added and samples were mixed by inverting six times. Samples were incubated for 3' then centrifuged at 4°C, 12,000xg, for 15'. Aqueous phase was transferred to a new tube and 350μL isopropanol was added. Samples were incubated at 4°C for 10' then centrifuged at 4°C, 12,000xg, for 10'. Supernatants were discarded and RNA was resuspended in 700μL of 75% EtOH, vortexed briefly, and centrifuged at 4°C, 7,500xg, for 5'. Supernatant was discarded and the pellets were allowed to air dry for 10' before resuspending in 20μL of water. A total of 0.4μL of DNase1 was added per sample and incubated at 37°C for 15'. DNase1 was inactivated at 75°C for 5'. Superscript IV (ThermoFisher, Cat# 18090010) procedure was used for reverse transcription of mRNA to cDNA. PowerUP SYBR Green master mix (ThermoFisher, Cat# A25741) was used for qPCR reactions using primers for controls and targeted regions within *loxP* sites of *Tbx2/3* (Supplemental File 1). StepOnePlus Real-Time PCR System was used to run qPCR assays.

2.9. Statistical Analysis

P-values for OV measurements and immunofluorescence cell counting was calculated using a Wilcoxon test. P-values of qRT-PCR results were calculated using a two tailed unpaired t-test. Means and standard error were plotted in graphs created using Prism 9 software. P-values for cluster proportions were calculated by performing two proportion Z tests.

3. Results

3.1. *Tbx2/3*cKO embryos have failed inner ear morphogenesis

To investigate the function of *Tbx2/3* in early mouse inner ear development, we used *Pax2-Cre* to drive recombination of *Tbx2* and *Tbx3* floxed alleles (*Tbx2/3*cKO; Fig. S1). Validation of knockdown of *Tbx2/3* transcripts was confirmed through semi-quantitative reverse transcriptase PCR and quantitative PCR (Fig. S1B–C, respectively). The phenotype of the inner ear of *Tbx2/3*cKO embryos was recently reported (Kaiser et al., 2021). However, since we planned to follow up with single cell analysis, we first validated their phenotypic findings in our mice by paint filling to visualize inner ear structures (E13.5; Fig. 1A–D) and H&E staining to observe cellular details (E13.5 and E15.5; Fig. 1C–F). We found that the OV of *Tbx2/3*cKO embryos failed to progress morphologically and did not develop mature inner ear structures, consistent with findings in the previous study (Kaiser et al., 2021).

Failure of inner ear morphogenesis could be due to changes in OV size, altered proliferation or apoptosis in the *Tbx2/3*cKO embryos. Interestingly, at E10.5, the OVs of the *Tbx2/3*cKO mutants were enlarged in the A-P axis, whilst remaining unchanged in the D-V and M-L

axes, suggesting that defects first arose around E10.5 (Fig. 1M). In the previous report, a thickening of the OV epithelium was detected, but we did not detect this change (Fig. S2), whereas they did not detect the expansion of the A-P axis. At this stage, we did not detect changes in rates of proliferation or apoptosis in the OV and CVG (Fig. 1I–J and N). In controls, there is a region of apoptosis in the ventral and dorsal domains of the OV (Fig. S2). In *Tbx2/3*cKO embryos, we did not observe the ventral apoptotic region found in controls however, we noted a region of apoptosis in the anteroventral OV (Fig. S2). The dorsal zone of apoptosis was the same in the control and mutant embryos (Fig. S2). This is in contrast to a previous report in which increased apoptosis overall was observed at E10.5 (Kaiser et al., 2021). The differences we observed could be due to differences in genetic background or differences in exact timing of the stages of the embryos. Increased apoptosis was detected one embryonic day later at E11.5 in the cochlear duct (Fig. 1K–L and O). We observed a cochlear defect in *Tbx2*cKO and *Pax2-Cre;Tbx2*$^{f/f}$*;Tbx3*$^{f/+}$ embryos (Fig. S3 and S4) that may result from excess apoptosis. *Tbx2/3*cKO, *Pax2-Cre;Tbx2*$^{f/f}$*;Tbx3*$^{f/+}$, and *Pax2-Cre;Tbx2*$^{f/+}$*;Tbx3*$^{f/f}$ phenotypes were further validated with *Pax8-Cre* (Fig. S4G–J). All genotypes and phenotypes from individual and combined *Tbx2/3*cKO embryos are provided (Fig. S3 and S4) but were not pursued further in this study.

3.2. Accumulation of otic progenitor cells and delayed differentiation in *Tbx2/3*cKO OVs identified by scRNA-seq

As a prelude to scRNA-seq, whole mount RNAscope (wmRNAscope) analysis of *Tbx2/3* expression was performed at E8.5-E10.5. Consistent with the previous study (Kaiser et al., 2021), *Tbx2* was expressed in the otic placode at E8.5 and throughout the OV at E10.5 with unique expression in the ventral and medial regions of the OV (Fig. 1R–S, arrowhead in 1S). *Tbx3* had low levels of expression at E9.0 in the otic cup and was dorsolaterally expressed at E10.5 with unique expression in the CVG (Fig. 1S, asterisk). Since both genes were strongly expressed at E10.5 and the earliest phenotype detected was at this stage, we selected E10.5 to perform scRNA-seq. This was done on two replicates of control (six OVs from three embryos, each) and *Tbx2/3*cKO (four OVs from two embryos, each) embryos. The OV with the CVG was microdissected from embryos with an effort to remove surrounding tissue. Individual GFP expressing cells were collected and purified by flow cytometry, and then used for scRNA-seq (Fig. S5).

Using the unbiased cell clustering feature in Seurat software, OV and CVG cells were identified in each individual sample with gene markers, *Oc90* encoding an otoconial protein and *Fbxo2,* encoding a protein for ubiquitination, for the OV as well as *NeuroD1* for the CVG (Fig. S6 and S6) (Hartman et al., 2015). Homeobox transcription factor genes, *Pax6* and *Phox2b* were used to identify cell populations in the neural tube (Carbe et al., 2013; Pla et al., 2008). Further, the transcription factor gene, *Twist1* was used to identify migrating neural crest cells (Fan et al., 2021). Homeodomain genes, *Hoxa2* and *Hoxb3,* were used to identify cells for cranial nerve VII and cranial nerve IX, respectively (Cordes, 2001). Marker genes identified for all clusters of each sample are provided (Supplemental File 3). We next performed subcluster analysis to resolve cell populations within the OV and CVG. This was carried out on each replicate of control and *Tbx2/3*cKO datasets using Seurat software, and UMAPs were generated to visualize different cell populations (Fig. S6 and S7). The

homeobox genes, *Dlx5, Dlx6, Otx1, Otx2,* and signaling gene, *Wnt2b* served as nonsensory markers (Morsli et al., 1999; Robledo & Lufkin, 2006; Sienknecht & Fekete, 2009). *Bmp4, Hey2, Fgf10, and Sox2* signaling genes were used as prosensory markers (Blauwkamp et al., 2007; Huh et al., 2012; S. Li et al., 2008). *Gata3, Fgf10, Eya1, Lfng,* and *Sox2,* were used as proneurosensory markers (Luo et al., 2013; Pauley et al., 2003; Wong et al., 2013). *NeuroD1* was used as a neural marker (Jahan et al., 2010) (Fig. S6 and S7). Other marker genes used to identify OV subclusters are provided (Fig. S6 and S7; Supplemental File 4).

To understand if cell fate progression was altered in *Tbx2/3*cKO embryos, the scRNA-seq data of the OV and CVG of each sample were processed separately through scVelo (Bergen et al., 2020) and CellRank (Lange et al., 2022) software. These software take advantage of the spliced and unspliced forms of mRNA that can be distinguished and used to generate estimation of the gene expression maturation state of cells. The cells are then ordered based on their estimated progression through cell fate (la Manno et al., 2018). The results were visualized in a directed Partition-based Graph Abstraction (PAGA) plot in which the initial and more differentiated terminal cellular states were identified per sample (Fig. 2A–B; Fig. S8). The PAGA plots were projected onto individual Seurat cell subcluster UMAPs (Fig. S6 and S7) to maintain consistent clustering throughout our analysis of individual samples (Fig. 2A–B; Fig. S8). The pie charts in the PAGA plots illustrated the fate potential of the different cell types. From the PAGA and UMAP plots, we identified similar initial and terminal states, but fewer branches to terminal states in *Tbx2/3*cKO embryos versus controls suggesting that the *Tbx2/3*cKO embryos may have not differentiated as far along as the controls (Fig. 2A–B; Fig. S8). The cells comprising the initial state were termed otic progenitor cells (gray in UMAP; Fig. 2A–B). There were three terminal states identified in each replicate and they coincided with the three main cell types of the inner ear, which are the prosensory, neural, and nonsensory cell types (Fig. 2A–B). Proneurosensory cells represented an intermediate state. We next generated circular projection plots from CellRank software to easily visualize how cells are progressing to each terminal state (Fig. 2A–B). Lack of progress to more differentiated states was apparent in *Tbx2/3*cKO OVs (lack of blue color at tips of circle projection, Fig. 2B) further suggesting that the cells in the *Tbx2/3*cKO embryos were less differentiated. These results were similar in both replicate experiments (Fig. S8).

Having gained some insights into the findings from analyzing individual samples, the four data sets comprising two control and two *Tbx2/3*cKO experiments were integrated using RISC software (Liu et al., 2021) (Fig. 2C). We identified changes in the distribution of cells in *Tbx2/3*cKO embryos in which there were relatively more cells in the center clusters and fewer cells in the outer clusters of the UMAP plot in *Tbx2/3*cKO embryos compared to controls (insert in Fig. 2C). This is consistent with changes in relative proportion of cell types in *Tbx2/3*cKO embryos (Fig. 2D). The central set of clusters with relatively more cells in *Tbx2/3*cKO embryos (Fig. 2C) were detected as cells of the initial state clusters in the PAGA plots of the individual data sets (Fig. 2A–B; Fig. S8) and identified as otic progenitor cells (clusters 4, 7, 8, 11; Fig. 2D; Fig. S9). Expression of individual gene markers of different terminal states as well as *Tbx2/3* are shown in Fig. 2E. As noted above, *Tbx2* was more widely expressed than *Tbx3*, while *Tbx3* was more widely expressed in the neural

cell types. Overall, the data is consistent with a failure in cell fate progression from otic progenitors to more differentiated states in *Tbx2/3*cKO mutant OVs.

3.3. Delayed progression of prosensory and nonsensory lineages in *Tbx2/3*cKO OVs

To further investigate changes in cell fate progression in *Tbx2/3*cKO OVs, we examined the probability of fate progression to each differentiated terminal state of prosensory, neural, and nonsensory cell types, for each cell per sample using CellRank software (Lange et al., 2022) and projected this onto the integrated RISC UMAP (Fig. 3A–C; Fig. S8). All three terminal states were affected with prosensory and nonsensory states having the greatest changes in *Tbx2/3*cKO OVs. The terminal state of the prosensory lineage retained an otic progenitor state as seen in the shift of the yellow cells to the otic progenitor cell clusters (Fig. 3A). This in concert with the results from the PAGA plots and circular projections (Fig. 2A–B; Fig. S8A–B) signifies that the terminal states in the *Tbx2/3*cKO samples are less mature and integrate to the less differentiated cell clusters of the control, which further suggested that they are immature. On the other hand, the nonsensory and neural cells had fewer differentiated cells as seen by a reduction of the relative amount of yellow cells (Fig. 3B–C). Some cells of the neural lineage were also present in the otic progenitor clusters, implying dysregulation of gene expression.

To examine gene expression differences that may be causing delayed differentiation between control and *Tbx2/3*cKO OVs, we further processed the scRNA-seq data through RISC software and identified DEGs. We also calculated lineage drivers for each terminal state through CellRank and plotted the genes that overlapped between the two sets of genes in a miniaturized heat map of the scaled expression of each gene vs developmental time as cells progress from initial to terminal states termed, latent time (Fig. 3D–F). The genes in the heat map were ordered based on their scaled expression (highest is in yellow) to give insight as to when lineage specific DEGs were expressed in terms of latent time. In the heat maps for prosensory and nonsensory lineages, many of the DEGs that were expressed as cells transitioned from their initial to terminal states in controls were expressed as terminal state genes in the OVs from *Tbx2/3*cKO embryos causing the terminal state of *Tbx2/3*cKO cells to mirror the transitioning intermediate states in control cells (Fig. 3D and F). This further suggests that the terminal states in the *Tbx2/3*cKO cells were not as mature as the terminal states of the control cells, and supports the findings presented above, that cells in mutant OVs failed to differentiate to their individual cell fates. We did not detect obvious differences in the heat map of the neural lineages.

Example lineage specific DEGs were plotted in graphs with expression versus latent time to better illustrate how the expression of genes that mark further differentiation of these cell lineages was delayed. These graphs plot the expression value from each cell along the path from initial to each terminal state. In the graphs for prosensory cells, *Bmp4*, *Gata2*, and *Gata3* showed delay in expression as detected as a shift to the right of the graph (Fig. 3D). Additionally, when these cells were co-clustered with the controls in the RISC integrated UMAPs, they clustered with the otic progenitors, further implicating their delay in maturation (Fig. 3A). These lineage DEGs were further investigated through wmRNAscope analysis. *Bmp4*, a gene crucial for prosensory lineage differentiation (Chang et al., 2008; H.

Li et al., 2005), was more diffusely localized in the anterior domain (Fig. 3G arrowhead) and expanded in the posterior domain of the OV (Fig. 3G asterisk), indicating significant changes in the patterning of the OV. Similarly, *Bmp4* expression was also changed in the UMAP plots, in which expression was slightly decreased in the prosensory domain (Fig. 3H arrowhead) and increased in the otic progenitor cells (Fig. 3H asterisk), suggesting consistency between methods. *Gata2* expression was reduced in the prosensory domains of the OV as observed in the wmRNAscope and feature plot images (Fig. S10A). *Gata3* expression was reduced in the prosensory domain and increased in the ventral region of the OV, consistent with UMAP results and suggesting that there was an accumulation of cells with *Gata3* expression in the otic progenitor populations (Fig. S10B). *Fgf10*, was expanded in the ventral and posterior domain of the OV and was expressed in otic progenitors in *Tbx2/3*cKO OVs (Fig. S10C). Due to dimension reduction afforded by scRNA-seq data, the localization of genes within the OV by wmRNAscope analysis was more complex than was indicated in the UMAPs.

The neural lineage cells were more mildly affected in mutant embryos as compared to the prosensory lineages, as detected by scRNA-seq and in the heat map as indicated above. Here, we found that expression of the three neural marker genes, *NeuroD1, Neurog1*, and *Rgs4* were delayed in the expression versus latent time plots (Fig. 3E). As previously reported (Kaiser et al., 2021), expression of *NeuroD1* was expanded into the posterior portion of the ventral OV (Fig. 3I). In contrast, neural clusters from scRNA-seq analysis were not expanded in *Tbx2/3*cKO embryos. However, *NeuroD1* was expressed in the otic progenitor cells, and perhaps this could explain the presence of more *NeuroD1* expressing cells, but of a different cell state (Fig. 3I–J).

The nonsensory domains were reduced in size as detected in the UMAPs (Fig. 3C) and representative genes, *Dlx5, Otx1*, and *Otx2* showed delayed or reduced expression in the latent time graphs (Fig. 3F). Expression of *Dlx5*, a marker of dorsal nonsensory cells, was reduced in the anterior domain of the OV as determined by wmRNAscope analysis. This is consistent with reduced expression observed in the UMAPs (Fig. 3L). Additionally, there was also expression of *Dlx5* in otic progenitor cells (Fig. 3K–L). The loss of expression in *Dlx5* was in the regions that overlapped prosensory domains of the OV in both the scRNA-seq and wmRNAscope data (Fig. 3K). The ventral expression domains of *Otx1* and *Otx2* were lost, with *Otx1* retaining some expression in the lateral OV (Fig. S10D–E), consistent with loss of cells in the ventral region in the UMAPs (Fig. 3C). Therefore, the ventral nonsensory domain was more dramatically affected than the dorsal nonsensory domain.

Examination of *Bmp4, NeuroD1, Dlx5*, and *Otx2* in the OVs in which two alleles of *Tbx3* and one allele of *Tbx2* was inactivated or vice versa, showed that inactivation of *Tbx2* led to more patterning defects, similar to *Tbx2/3*cKO OVs (Fig. S11A–L). This is consistent with the wider expression domain of *Tbx2* (above).

3.4. Otic progenitor cell population was expanded in the OV of *Tbx2/3*cKO embryos

We next wanted to identify marker genes of the otic progenitor cells and determine their location in the OV by wmRNAscope analysis. Otic progenitor (gray tones; clusters 4,

7, 8 and 11), prosensory (pink tones; clusters 5 and 9), neural (yellow tones; clusters 2 and 6), proneurosensory (green, cluster 3) and nonsensory (blue tones; clusters 1, 10, 12, 13) clusters were consolidated separately (Fig. 4A). Cell fate progression of initial developmental states in otic progenitor cells to the three main inner ear cell types are indicated in Fig. 4A, while the relative proportions of each group is shown in Fig. 4B. The otic progenitors constituted a relatively low proportion of cells in controls but had a three-fold increase in proportion in *Tbx2/3*cKO OVs (Fig. 4B and Supplemental File 5). The increased proportion of otic progenitor cells in *Tbx2/3*cKO was followed by a reduction in the proportion of neural, proneurosensory, prosensory and nonsensory cells. We then identified and examined expression of markers of otic progenitors. The genes, *Fgf18, Cxcl12, Sox3*, and *Pou3f3* are representative markers for the otic progenitors and are also DEGs in *Tbx2/3*cKO embryos (Supplemental File 6 and 7). *Fgf18* was expressed very slightly in the medioventral domain of control OVs, but its expression was expanded throughout the ventral region of the OV in *Tbx2/3*cKO embryos (Fig. 4C; and insert of digital sections; see larger size in Fig. S12A). This is consistent with expression of three other marker genes, *Cxcl12, Sox3*, and *Pou3f3* (Fig. 4D–F; large sized digital sections in Fig. S12B–D). Expression of *Sox3* and *Pou3f3* was also encroaching on the dorsal half of the OV (Fig. 4E–F; Fig. S12C–D). Similar findings were observed with known otic markers *Eya1, Six1*, and *Sox2* that generally have broader expression domains but were also expressed in otic progenitor cells in *Tbx2/3*cKO embryos (Fig. S10F–H; Fig. S12E–F). Their expression in the posterior dorsal prosensory domain overlapped with the expanded *Bmp4* expression (Fig. 3G).

We next generated a co-expression heat map of marker genes within the otic progenitor cells (initial state) versus cells in the proneurosensory (intermediate), prosensory, neural, and nonsensory (terminal states) cells in integrated scRNA-seq data of control versus *Tbx2/3*cKO OVs (Fig. 4G). As above, *Fgf18, Sox3, Cxcl12*, and *Pou3f3* are marker genes of otic progenitor cells; *Cxcl12* and *Pou3f3* were also expressed in some proneurosensory cells. Marker genes of other cell types were also expressed at low levels in otic progenitor cells in controls. In contrast in *Tbx2/3*cKO embryos, genes from other terminal populations were expressed in otic progenitor cells. For example, the proneurosensory marker gene (*Fgf10*) and neural marker genes (*Neurog1* and *NeuroD1*; Fig. 4G; Fig. S13) were detected in otic progenitor cells, which might explain why there is ectopic neural cells in the posterior ventral OV in *Tbx2/3*cKO embryos. We found that several *Fgf* genes were expressed in the expanded otic progenitor population (e.g. *Fgf10, Fgf18*), suggesting that there is upregulation of FGF signaling in the mutant embryos (Supplemental File 6 and 7). There was also reduced expression of prosensory and nonsensory marker genes in mutant embryos, demonstrating reduced expression among fewer cells (Fig. 4G). Overall, this data is consistent with the possibility that otic progenitors are a source of multipotent cells in the OV needed to progress to more differentiated states at a key developmental time during which the OV begins to undergo morphological changes to form inner ear organs. When *Tbx2/3* are inactivated, the otic progenitors accumulate along with dysregulation of gene expression leading to fewer cells differentiating properly.

3.5. Dysregulation of *Neurog1* and *NeuroD1* leads to an ectopic zone of neurogenesis in *Tbx2/3*cKO OVs

To understand why there is a duplicated CVG but yet the neural cell clusters from scRNA-seq data were not enlarged, we compared the expression pattern of *Neurog1/NeuroD1* in the OV, with that of *Rgs4* that is expressed in more mature delaminated neurons (Kim et al., 2014). Surprisingly, we did not observe an expansion of *Rgs4* expression in the CVG in the posterior region of the OV where *Neurog1* was ectopically expressed (Fig. 5). We also noted that *Neurog1* expression was detected in the otic progenitor cells (Fig. 5B, arrow) as was *NeuroD1* (Fig. 3H, arrow). The significant increase in the number of cells expressing *Neurog1* and *NeuroD1* were quantified and shown in Fig. S13A. There were also cells with overlapping expression of both *Neurog1* and *NeuroD1* in the posterior OV where *Rgs4* was not expressed (Fig. 5A; Fig. S13B). This further supports that the cells in the posterior OV, of which some are delaminating (Fig. S13B), are immature and in an otic progenitor cell state (lime green color in model in Fig. 5B, arrow).

We also further investigated *NeuroD1* and *Neurog1* expression at E9.5 to identify if at an early stage, these genes were ectopically expressed in the posterior OV. Interestingly, they were restricted to the anterior region of the OV as they are in controls at this stage (Fig. 5C). Thus, the defects in patterning of the OV occurred in multipotent otic progenitor cells after the axes have formed and initial patterning has taken place.

4. Discussion

In this report we identified a multipotent otic progenitor cell population that provides a continuous source of precursors needed for morphogenesis of inner ear cell types in the OV. From scRNA-seq analysis of *Tbx2/3*cKO embryos at E10.5, we found a three-fold expansion of otic progenitor cells to the detriment of more differentiated states in the absence of changes in rates of proliferation or apoptosis. We additionally found dysregulation of gene expression in otic progenitors, including that of *Neurog1* and *NeuroD1.* We suggest that these cells may contribute to the ectopic zone of neurogenesis in the posterior OV in mutant embryos. Overall, *Tbx2/3* may function to restrict self-renewal of the otic progenitor population and gene expression within, thereby promoting differentiation.

4.1 Model of inner ear development and disruption by loss of *Tbx2/3*

A model for inner ear development is shown in Fig. 6. In this model, the main axes of the inner ear are indicated (black lines in Fig. 6A–B). These axes are established during the early otic placode to early otic vesicle stages of inner ear development. Once axes are established, the compartmentalized OV expresses genes that mark prosensory (pink), neural (orange), and nonsensory (turquoise) cell lineages (Fig. 6A, 6C). We now identified otic progenitor cells (*Fgf18, Sox3, Cxcl12*; gray color) that may function at E10.5, upstream of proneurosensory cells (*Eya1, Six1*; light green; Fig. 6A, 6C). These otic progenitors, may contribute cells to the three main cell type lineages as shown in the model of cell fate specification (Fig. 6A, 6C; green arrows, for increase in cell number; red arrows for decreased expression). From the data presented in this report, we suggest that *Tbx2/3* functions to promote fate progression of otic progenitor population, while

restricting ectopic gene expression (Fig. 4, summarized in Fig. 6B; 6D). From analysis of expression of otic progenitor markers versus latent time (Fig. S14 summarized in Fig. 6E–F) the data is consistent with delayed differentiation to more terminal states and expansion otic progenitors in *Tbx2/3*cKO OVs. We did not observe increased rates of proliferation or apoptosis at E10.5. We suggest that the relative excess in otic progenitors is due to failure of cells to progress to more mature states resulting in cell accumulation, rather than more cell division. *Tbx2/3* are widely expressed in the OV and function as transcriptional repressors in many developmental contexts (Farin et al., 2013; Lüdtke et al., 2016; Mesbah et al., 2012; Suzuki et al., 2004; Zirzow et al., 2009). Therefore, we suggest that *Tbx2/3* may directly or indirectly repress expression of genes in otic progenitors.

The zone of neurogenesis was expanded in the OV and neural progenitor cells delaminated from the posterior ventral region in *Tbx2/3*cKO embryos, yet the relative number of cells in neuronal clusters from scRNA-seq experiments were not increased. It is possible that the ectopic zone of neurogenesis is a result of dysregulated gene expression in otic progenitor cells. The otic progenitors in control and *Tbx2/3*cKO embryos expressed *Eya1* and *Six1* at E10.5 (Fig. 6C–D). EYA1 and SIX1 form transcriptional activation protein complexes (Wong et al., 2013) and have important functions in directing neurogenesis and promoting neural differentiation in the OV (Ahmed et al., 2012). We found that *Eya1* and *Six1* were broadly expressed in otic progenitors in control and *Tbx2/3*cKO embryos. We observed delayed expression of *Eya1* and *Six1* in the more differentiated, terminal states of the OV (Fig. S14, summarized in Fig. 6C–D). This is consistent with continued expression of neural markers, *Neurog1* and *NeuroD1*, in the otic progenitor cells, as *Eya1-Six1* act upstream of proneurosensory markers, *Fgf10* and *Gata3* to promote neurogenesis (Zou et al., 2006). *Fgf10* and *Gata3* were expressed in otic progenitor cells in *Tbx2/3*cKO embryos and these might act upstream of ectopic expression of *Neurog1* and *NeuroD1.* It was recently shown that *Tbx2/3* are required upstream of FGF signaling in the OV to restrict neural development (Kaiser et al., 2021). In our report, many *Fgf* genes (e.g. *Fgf10* and *Fgf18*) were expressed in the expanded otic progenitor population, consistent with upregulation of FGF signaling in the mutant embryos (Supplemental File 6 and 7). This increase in FGF signaling could also explain the observed alterations of gene expression and morphogenesis of the OV, including *Neurog1* and *NeuroD1. Sox3* encodes a homeodomain transcription factor and is one of the marker genes for otic progenitor cells that is a downstream target of *Fgf8* and promotes neurogenesis (Evsen et al., 2013; Kaiser et al., 2021). It is possible that *Sox3* plays an important role in this progression. When taken together, delayed maturation by gene dysregulation of otic progenitor cells from loss of *Tbx2/3* disrupts morphogenesis of the OV.

4.2 *Tbx2* and *Tbx3* potential functions in regulating signaling required for morphogenesis.

In addition to the FGF signaling discussed above, there are additional signals in the OV that may act downstream of *Tbx2/3*. We have shown that *Tbx2/3* are required for the proper differentiation of cells as they progress from otic progenitor to prosensory and nonsensory cell fates. Both the prosensory and nonsensory cell fates are dependent on the WNT/Sonic hedgehog (SHH) signaling gradients (Żak & Daudet, 2021). This was demonstrated by a reduction of *Dlx5* expression in the dorsal region (Fig. 3K) and loss of *Otx2* in the ventral

region of the OV in *Tbx2/3*cKO embryos (Fig. S10D). These two genes have been shown to function downstream of WNT and SHH signaling respectively (Rakowiecki et al., 2013; Riccomagno et al., 2002b, 2005). Furthermore, some *Wnt* related genes were dysregulated in the scRNA-seq data from *Tbx2/3*cKO mutant embryos, such as *Wnt2b, Wnt4*, and *Wnt5a.* Additionally, some SHH related genes were also dysregulated in the *Tbx2/3*cKO mutant embryos such as *Gli1, Sufu*, and *Kif7* (Supplemental File 7). This suggests that *Tbx2/3* may regulate these signaling pathways during the development of the inner ear. Another signaling pathway that is important for specifying the anterior-posterior axis of the inner ear is retinoic acid (RA) that has been shown to function upstream *Tbx1* (Bok, Raft, Kong, Koo, Dräger, et al., 2011) and is required for the restriction of the neurogenic domain of the OV. It is possible that *Tbx2/3* functions to maintain the RA signal within the OV as some RA genes were dysregulated such as *Rdh10, Aldh1a2*, and *Cyp26a1* (Supplemental File 7). Future studies will shed light onto the potential functions of *Tbx2/3* in these signaling pathways.

4.3 Strengths and limitations of integrating whole mount in situ hybridization and single cell analyses

In this report, we gained insights into the shared early functions of *Tbx2/3* by performing single cell transcriptomics. Unfortunately, this method does not provide spatial insights into gene expression changes. We attempted to gain spatial insights and validate gene expression changes using wmRNAscope *in situ* hybridization methods. However, wmRNAscope analysis provided spatial but not quantitative insights. Therefore, both techniques have strengths and limitations. By scRNA-seq analysis, we identified an expanded otic progenitor population of which some cells expressed *Neurog1* and *NeuroD1*, and reduced prosensory and nonsensory populations (Fig. 6). The wmRNAscope analysis enabled us to localize the otic progenitor population (Fig. 4, summarized in Fig. 6). We found that the anterior and posterior prosensory domains were difficult to differentiate from one another in the scRNA-seq data, but these were discerned in the wmRNAscope data. Further, we identified an ectopic zone of neurogenesis in the posterior OV by wmRNAscope analysis, but by single cell RNA-seq analysis, the main differences in the mutant embryos were a relative sparing of the neurogenesis domain co-occurring with an increase of expression in the otic progenitor population. Understanding the role of otic progenitor cells using techniques in the future, such as spatial transcriptomics will provide single cell resolution in spatial context. Further, we may gain insights in mechanisms of gene regulation by identifying changes in chromatin accessibility on a single cell level in the context of RNA changes.

Conclusions

Overall, we identified a population of otic progenitor cells that are restricted in size by *Tbx2/3* during morphogenesis of the OV to form the main cell types in the inner ear. These otic progenitor cells, expressing marker genes, are largely localized to the ventral domain of the OV. Inactivation of *Tbx2/3* leads to an accumulation of these otic progenitor cells along with disruption of patterning observed by *in situ* analysis in embryos. This provides new insights, at a single cell level, into the normal developmental processes that take place to form the inner ear and explains the molecular basis of the phenotypes that occurred in *Tbx2/3*cKO embryos.

Supplementary Material

Refer to Web version on PubMed Central for supplementary material.

Acknowledgements

We thank Dr. Lu Zhang and Dr. Chenleng Cai for the generation of the *Tbx2/3* floxed mice. We appreciate mentorship and helpful suggestions on this project from Dr. Pin-Xian Xu at Icahn School of Medicine at Mount Sinai, NY. We thank Dr. Christopher De Bono for scientific discussion and support in optimizing many of the experiments used in this study. We thank Dr. Deyou Zheng, Dr. Yang Liu, and Alexander Ferrena for scientific discussion and advice for bioinformatic analysis. We thank Dr. Andrew K. Groves for providing the *Pax2-Cre* mice. We thank the Genomics core, especially David Reynolds, Director of the Genomics Core, Shahina Maqbool, Director of the Flow Cytometry facilities at Einstein. We thank the Analytical Imaging Facility, especially Andrea Briceno and Hillary Guzik, funded by NCI Cancer Center Support Grant P30CA013330. We would like to thank Dr. Charles Query, Director of the Training Program in Cellular and Molecular Biology and Genetics, 5T32GM007491, for supporting the work of Hansoo Song. The work was also funded by the NIDCD, NIH Ruth L. Kirschstein National Research Service Award (NRSA) Individual Predoctoral Fellowship (Parent F31), F31DC019037.

Data Availability

The scRNA-seq data sets from this study (accession number GSE185172) are available on NCBI Gene Expression Omnibus (GEO; https://www.ncbi.nlm.nih.gov/geo/).

References:

Adam J, Myat A, le Roux I, Eddison M, Henrique D, Ish-Horowicz D, & Lewis J (1998). Cell fate choices and the expression of Notch, Delta and Serrate homologues in the chick inner ear: parallels with Drosophila sense-organ development. Development (Cambridge, England), 125(23), 4645–4654. 10.1242/dev.125.23.4645 [PubMed: 9806914]

Ahmed M, Xu J, & Xu PX (2012). EYA1 and SIX1 drive the neuronal developmental program in cooperation with the SWI/SNF chromatin-remodeling complex and SOX2 in the mammalian inner ear. Development, 139(11), 1965–1977. 10.1242/dev.071670 [PubMed: 22513373]

Bergen V, Lange M, Peidli S, Wolf FA, & Theis FJ (2020). Generalizing RNA velocity to transient cell states through dynamical modeling. Nature Biotechnology, 38(12), 1408–1414. 10.1038/s41587-020-0591-3

Blauwkamp MN, Beyer LA, Kabara L, Takemura K, Buck T, King WM, Dolan DF, Barald KF, Raphael Y, & Koenig RJ (2007). The role of bone morphogenetic protein 4 in inner ear development and function. Hearing Research, 225(1–2), 71–79. 10.1016/j.heares.2006.12.010 [PubMed: 17275231]

Bok J, Chang W, & Wu DK (2007). Patterning and morphogenesis of the vertebrate inner ear. The International Journal of Developmental Biology, 51(6–7), 521–533. 10.1387/ijdb.072381jb [PubMed: 17891714]

Bok J, Raft S, Kong K-A, Koo SK, Drager UC, & Wu DK (2011). Transient retinoic acid signaling confers anterior-posterior polarity to the inner ear. Proceedings of the National Academy of Sciences, 108(1), 161–166. 10.1073/pnas.1010547108

Bouchard M, Souabni A, & Busslinger M (2004). Tissue-specific expression of ere recombinase from thePax8 locus. Genesis, 38(3), 105–109. 10.1002/gene.20008 [PubMed: 15048807]

Carbe C, Garg A, Cai Z, Li H, Powers A, & Zhang X (2013). An Allelic Series at the Paired Box Gene 6 (Pax6) Locus Reveals the Functional Specificity of Pax Genes. Journal of Biological Chemistry, 288(17), 12130–12141. 10.1074/JBC.M112.436865 [PubMed: 23515312]

Chang W, Lin Z, Kulessa H, Hebert J, Hogan BLM, & Wu DK (2008). Bmp4 Is Essential for the Formation of the Vestibular Apparatus that Detects Angular Head Movements. PLoS Genetics, 4(4), e1000050. 10.1371/journal.pgen.1000050 [PubMed: 18404215]

Chatterjee S, Kraus P, & Lufkin T (2010). A symphony of inner ear developmental control genes. BMC Genetics, 11(1), 68. 10.1186/1471-2156-11-68 [PubMed: 20637105]

Cole LK, le Roux I, Nunes F, Laufer E, Lewis J, & Wu DK (2000). Sensory organ generation in the chicken inner ear: contributions of bone morphogenetic protein 4, serratel, and lunatic fringe. The Journal of Comparative Neurology, 424(3), 509–520. 10.1002/1096-9861(20000828)424:3<509::aid-cne8>3.0.co;2-q [PubMed: 10906716]

Coll M, Seidman JG, & Müller CW (2002). Structure of the DNA-bound T-box domain of human TBX3, a transcription factor responsible for ulnar-mammary syndrome. Structure (London, England: 1993), 10(3), 343–356. http://www.ncbi.nlm.nih.gov/pubmed/12005433 [PubMed: 12005433]

Cordes SP (2001). Molecular genetics of cranial nerve development in mouse. Nature Reviews Neuroscience, 2(9), 611–623. 10.1038/35090039 [PubMed: 11533729]

Duncan JS, & Fritzsch B (2013). Continued expression of GATA3 is necessary for cochlear neurosensory development. PloS One, 8(4), e62046. 10.1371/journal.pone.0062046 [PubMed: 23614009]

Durruthy-Durruthy R, Gottlieb A, Hartman BH, Waldhaus J, Laske RD, Altman R, & Heller S (2014). Reconstruction of the mouse otocyst and early neuroblast lineage at single-cell resolution. Cell, 157(4), 964–978. 10.1016/j.cell.2014.03.036 [PubMed: 24768691]

Economou A, Datta P, Georgiadis V, Cadot S, Frenz D, & Maconochie M (2013). Gata3 directly regulates early inner ear expression of Fgf10. Developmental Biology, 374(1), 210–222. 10.1016/j.ydbio.2012.11.028 [PubMed: 23220102]

Evsen L, Sugahara S, Uchikawa M, Kondoh H, & Wu DK (2013). Progression of neurogenesis in the inner ear requires inhibition of Sox2 transcription by neurogenin1 and neurod1. The Journal of Neuroscience : The Official Journal of the Society for Neuroscience, 33(9), 3879–3890. 10.1523/JNEUROSCI.4030-12.2013 [PubMed: 23447599]

Fan X, Masamsetti VP, Sun JQ, Engholm-Keller K, Osteil P, Studdert J, Graham ME, Fossat N, & Tam PP (2021). TWIST1 and chromatin regulatory proteins interact to guide neural crest cell differentiation. ELife, 10. 10.7554/eLife.62873

Farin HF, Lüdtke TH-W, Schmidt MK, Placzko S, Schuster-Gossler K, Petry M, Christoffels VM, & Kispert A (2013). Tbx2 Terminates Shh/Fgf Signaling in the Developing Mouse Limb Bud by Direct Repression of Gremlin1. PLoS Genetics, 9(4), e1003467. 10.1371/journal.pgen.1003467 [PubMed: 23633963]

Freyer L, & Morrow BE (2010). Canonical Wnt signaling modulates Tbx1, Eya1, and Six1 expression, restricting neurogenesis in the otic vesicle. Developmental Dynamics, 239(6), 1708–1722. 10.1002/dvdy.22308 [PubMed: 20503367]

Friedman RA, Makmura L, Biesiada E, Wang X, & Keithley EM (2005). Eya1 acts upstream of Tbx1, Neurogenin 1, NeuroD and the neurotrophins BDNF and NT-3 during inner ear development. Mechanisms of Development, 122(5), 625–634. 10.1016/j.mod.2004.12.011 [PubMed: 15817220]

Hartman BH, Durruthy-Durruthy R, Laske RD, Losorelli S, & Heller S (2015). Identification and characterization of mouse otic sensory lineage genes. Frontiers in Cellular Neuroscience, 9, 79. 10.3389/fncel.2015.00079 [PubMed: 25852475]

Huh S-H, Jones J, Warchol ME, & Ornitz DM (2012). Differentiation of the Lateral Compartment of the Cochlea Requires a Temporally Restricted FGF20 Signal. PLoS Biology, 10(1), e1001231. 10.1371/journal.pbio.1001231 [PubMed: 22235191]

Jahan I, Kersigo J, Pan N, & Fritzsch B (2010). Neurod1 regulates survival and formation of connections in mouse ear and brain. Cell and Tissue Research, 341(1), 95–110. 10.1007/S00441-010-0984-6 [PubMed: 20512592]

Kaiser M, Wojahn I, Rudat C, Lüdtke TH, Christoffels VM, Moon A, Kispert A, & Trowe M-O (2021). Regulation of otocyst patterning by Tbx2 and Tbx3 is required for inner ear morphogenesis in the mouse. Development (Cambridge, England), 148(8). 10.1242/dev.195651

Kiernan AE, Pelling AL, Leung KKH, Tang ASP, Bell DM, Tease C, Lovell-Badge R, Steel KP, & Cheah KSE (2005). Sox2 is required for sensory organ development in the mammalian inner ear. Nature, 434(7036), 1031–1035. 10.1038/nature03487 [PubMed: 15846349]

Kim HJ, Ryu J, Woo H-M, Cho SS, Sung MK, Kim SC, Park M-H, Park T, & Koo SK (2014). Patterns of Gene Expression Associated with Pten Deficiency in the Developing Inner Ear. PLoS ONE, 9(6), e97544. 10.1371/journal.pone.0097544 [PubMed: 24893171]

la Manno G, Soldatov R, Zeisel A, Braun E, Hochgerner H, Petukhov V, Lidschreiber K, Kastriti ME, Lönnerberg P, Furlan A, Fan J, Borm LE, Liu Z, van Bruggen D, Guo J, He X, Barker R, Sundström E, Castelo-Branco G, … Kharchenko P. v. (2018). RNA velocity of single cells. Nature, 560(7719), 494–498. 10.1038/S41586-018-0414-6 [PubMed: 30089906]

Lange M, Bergen V, Klein M, Setty M, Reuter B, Bakhti M, Lickert H, Ansari M, Schniering J, Schiller HB, Pe'er D, &Theis FJ (2022). CellRank for directed single-cell fate mapping. Nature Methods, 19(2), 159–170. 10.1038/s41592-021-01346-6 [PubMed: 35027767]

Li H, Corrales CE, Wang Z, Zhao Y, Wang Y, Liu H, & Heller S (2005). BMP4 signaling is involved in the generation of inner ear sensory epithelia. BMC Developmental Biology, 5(1), 16. 10.1186/1471-213X-5-16 [PubMed: 16107213]

Li S, Mark S, Radde-Gallwitz K, Schlisner R, Chin MT, & Chen P (2008). Hey2 functions in parallel with Hes1 and Hes5 for mammalian auditory sensory organ development. BMC Developmental Biology, 8, 20. 10.1186/1471-213X-8-20 [PubMed: 18302773]

Lilleväli K, Haugas M, Matilainen T, Pussinen C, Karis A, & Salminen M (2006). Gata3 is required for early morphogenesis and Fgf10 expression during otic development. Mechanisms of Development, 123(6), 415–429. 10.1016/J.MOD.2006.04.007 [PubMed: 16806848]

Lin Z, Cantos R, Patente M, & Wu DK (2005). Gbx2 is required for the morphogenesis of the mouse inner ear: a downstream candidate of hindbrain signaling. Development (Cambridge, England), 132(10), 2309–2318. 10.1242/dev.01804 [PubMed: 15829521]

Liu Y, Wang T, Zhou B, & Zheng D (2021). Robust integration of multiple single-cell RNA sequencing datasets using a single reference space. Nature Biotechnology, 39(7), 877–884. 10.1038/s41587-021-00859-x

Lüdtke TH, Rudat C, Wojahn I, Weiss A-C, Kleppa M-J, Kurz J, Farin HF, Moon A, Christoffels VM, & Kispert A (2016). Tbx2 and Tbx3 Act Downstream of Shh to Maintain Canonical Wnt Signaling during Branching Morphogenesis of the Murine Lung. Developmental Cell, 39(2), 239–253. 10.1016/j.devcel.2016.08.007 [PubMed: 27720610]

Luo X, Deng M, Xie X, Huang L, Wang H, Jiang L, Liang G, Hu F, Tieu R, Chen R, & Gan L (2013). GATA3 controls the specification of prosensory domain and neuronal survival in the mouse cochlea. Human Molecular Genetics, 22(18), 3609–3623. 10.1093/hmg/ddt212 [PubMed: 23666531]

Ma Q, Anderson DJ, & Fritzsch B (2000). Neurogenin 1 Null Mutant Ears Develop Fewer, Morphologically Normal Hair Cells in Smaller Sensory Epithelia Devoid of Innervation. 1(2). 10.1007/s101620010017

Ma Q, Chen Z, Barrantes IDB, De La Pompa JL, Anderson DJ, del Barco Barrantes I, De La Pompa JL, & Anderson DJ (1998). neurogenin1 is essential for the determination of neuronal precursors for proximal cranial sensory ganglia. Neuron, 20(3), 469–482. 10.1016/S0896-6273(00)80988-5 [PubMed: 9539122]

Mesbah K, Rana MS, Francou A, van Duijvenboden K, Papaioannou VE, Moorman AF, Kelly RG, & Christoffels VM (2012). Identification of a Tbx1/Tbx2/Tbx3 genetic pathway governing pharyngeal and arterial pole morphogenesis. Human Molecular Genetics, 21(6), 1217–1229. 10.1093/hmg/ddr553 [PubMed: 22116936]

Morrison A, Hodgetts C, Gossler A, Hrabé de Angelis M, & Lewis J (1999). Expression of Delta1 and Serrate1 (Jagged1) in the mouse inner ear. Mechanisms of Development, 84(1–2), 169–172. 10.1016/s0925-4773(99)00066-0 [PubMed: 10473135]

Morsli H, Choo D, Ryan A, Johnson R, & Wu DK (1998). Development of the mouse inner ear and origin of its sensory organs. The Journal of Neuroscience : The Official Journal of the Society for Neuroscience, 18(9), 3327–3335. http://www.ncbi.nlm.nih.gov/pubmed/9547240 [PubMed: 9547240]

Morsli H, Tuorto F, Choo D, Postiglione MP, Simeone A, & Wu DK (1999). Otx1 and Otx2 activities are required for the normal development of the mouse inner ear. Development, 126(11).

Ohyama T, Basch ML, Mishina Y, Lyons KM, Segil N, & Groves AK (2010). BMP signaling is necessary for patterning the sensory and nonsensory regions of the developing mammalian cochlea. The Journal of Neuroscience : The Official Journal of the Society for Neuroscience, 30(45), 15044–15051. 10.1523/JNEUROSCI.3547-10.2010 [PubMed: 21068310]

Ohyama T, & Groves AK (2004). Generation of Pax2-Cre mice by modification of a Pax2 bacterial artificial chromosome. Genesis, 38(4), 195–199. 10.1002/gene.20017 [PubMed: 15083520]

Ozaki H, Nakamura K, Funahashi J, Ikeda K, Yamada G, Tokano H, Okamura H, Kitamura K, Muto S, Kotaki H, Sudo K, Horai R, Iwakura Y, & Kawakami K (2004). Six1 controls patterning of the mouse otic vesicle. Development (Cambridge, England), 131(3), 551–562. 10.1242/dev.00943 [PubMed: 14695375]

Papaioannou VE (2014). The T-box gene family: emerging roles in development, stem cells and cancer. Development, 141(20), 3819–3833. 10.1242/dev.104471 [PubMed: 25294936]

Pauley S, Wright TJ, Pirvola U, Ornitz D, Beisel K, & Fritzsch B (2003). Expression and function of FGF10 in mammalian inner ear development. Developmental Dynamics, 227(2), 203–215. 10.1002/dvdy.10297 [PubMed: 12761848]

Pla P, Hirsch M-R, le Crom S, Reiprich S, Harley VR, & Goridis C (2008). Identification of Phox2b-regulated genes by expression profiling of cranial motoneuron precursors. Neural Development, 3(1), 14. 10.1186/1749-8104-3-14 [PubMed: 18565209]

Raft S, & Groves AK (2015). Segregating neural and mechanosensory fates in the developing ear: patterning, signaling, and transcriptional control. Cell and Tissue Research, 359(1), 315–332. 10.1007/s00441-014-1917-6 [PubMed: 24902666]

Rakowiecki S, Epstein DJ, Waring MT, Riedl AE, Garcia LF, McMahon AP, Sommer L, Boussadia O, & Kemler R (2013). Divergent roles for Wnt/βcatenin signaling in epithelial maintenance and breakdown during semicircular canal formation. Development (Cambridge, England), 140(8), 1730–1739. 10.1242/dev.092882 [PubMed: 23487315]

Riccomagno MM, Martinu L, Mulheisen M, Wu DK, & Epstein DJ (2002a). Specification of the mammalian cochlea is dependent on Sonic hedgehog. Genes & Development, 16(18), 2365–2378. 10.1101/gad.1013302 [PubMed: 12231626]

Riccomagno MM, Martinu L, Mulheisen M, Wu DK, & Epstein DJ (2002b). Specification of the mammalian cochlea is dependent on Sonic hedgehog. Genes & Development, 16(18), 2365–2378. 10.1101/gad.1013302 [PubMed: 12231626]

Riccomagno MM, Takada S, & Epstein DJ (2005). Wnt-dependent regulation of inner ear morphogenesis is balanced by the opposing and supporting roles of Shh. Genes & Development, 19(13), 1612–1623. 10.1101/gad.1303905 [PubMed: 15961523]

Robledo RF, & Lufkin T (2006). Dlx5 and Dlx6 homeobox genes are required for specification of the mammalian vestibular apparatus. Genesis, 44(9), 425–437. 10.1002/dvg.20233 [PubMed: 16900517]

Schlosser G, Awtry T, Brugmann SA, Jensen ED, Neilson K, Ruan G, Stammler A, Voelker D, Yan B, Zhang C, Klymkowsky MW, & Moody SA (2008). Eya1 and Six1 promote neurogenesis in the cranial placodes in a SoxB1-dependent fashion. Developmental Biology, 320(1), 199–214. 10.1016/j.ydbio.2008.05.523 [PubMed: 18571637]

Sienknecht UJ, & Fekete DM (2009). Mapping of Wnt, frizzled, and Wnt inhibitor gene expression domains in the avian otic primordium. The Journal of Comparative Neurology, 517(8), 751–764. 10.1002/cne.22169 [PubMed: 19842206]

Sousa VH, Miyoshi G, Hjerling-Leffler J, Karayannis T, & Fishell G (2009). Characterization of Nkx6-2-derived neocortical interneuron lineages. Cerebral Cortex (New York, N.Y.: 1991), 19 Suppl 1(Suppl 1), i1–10. 10.1093/cercor/bhp038 [PubMed: 19363146]

Suzuki T, Takeuchi J, Koshiba-Takeuchi K, & Ogura T (2004). Tbx Genes Specify Posterior Digit Identity through Shh and BMP Signaling. Developmental Cell, 6(1), 43–53. http://www.ncbi.nlm.nih.gov/pubmed/14723846 [PubMed: 14723846]

Torres M, & Giráldez F (1998). The development of the vertebrate inner ear. Mechanisms of Development, 71(1–2), 5–21. 10.1016/S0925-4773(97)00155-X [PubMed: 9507049]

Whitfield TT, & Hammond KL (2007). Axial patterning in the developing vertebrate inner ear. The International Journal of Developmental Biology, 51(6–7), 507–520. 10.1387/ijdb.072380tw [PubMed: 17891713]

Wong EYM, Ahmed M, & Xu P-X (2013). EYA1-SIX1 complex in neurosensory cell fate induction in the mammalian inner ear. Hearing Research, 297, 13–19. 10.1016/j.heares.2012.09.009 [PubMed: 23104013]

Wu DK, Nunes FD, & Choo D (1998). Axial specification for sensory organs versus non-sensory structures of the chicken inner ear. Development (Cambridge, England), 125(1), 11–20. http://www.ncbi.nlm.nih.gov/pubmed/9389659 [PubMed: 9389659]

Wu DK, & Oh SH (1996). Sensory organ generation in the chick inner ear. The Journal of Neuroscience : The Official Journal of the Society for Neuroscience, 16(20), 6454–6462. 10.1523/JNEUROSCI.16-20-06454.1996 [PubMed: 8815924]

Żak M, & Daudet N (2021). A gradient of Wnt activity positions the neurosensory domains of the inner ear. ELife, 10. 10.7554/eLife.59540

Zhang T, Xu J, Maire P, & Xu PX (2017). Six1 is essential for differentiation and patterning of the mammalian auditory sensory epithelium. PLoS Genetics, 13(9), e1006967. 10.1371/journal.pgen.1006967 [PubMed: 28892484]

Zheng W, Huang L, Wei Z-B, Silvius D, Tang B, & Xu P-X, (2003). The role of Six1 in mammalian auditory system development. Development (Cambridge, England), 130(17), 3989–4000. 10.1242/dev.00628 [PubMed: 12874121]

Zirzow S, Lüdtke TH-W, Brons JF, Petry M, Christoffels VM, & Kispert A (2009). Expression and requirement of T-box transcription factors Tbx2 and Tbx3 during secondary palate development in the mouse. Developmental Biology, 336(2), 145–155. 10.1016/J.YDBIO.2009.09.020 [PubMed: 19769959]

Zou D, Silvius D, Rodrigo-Blomqvist S, Enerbäck S, & Xu P-X (2006). Eya1 regulates the growth of otic epithelium and interacts with Pax2 during the development of all sensory areas in the inner ear. Developmental Biology, 298(2), 430–441. 10.1016/j.ydbio.2006.06.049 [PubMed: 16916509]

Highlights

- Single-cell RNA sequencing reveals otic progenitor cells in otic vesicle (OV)
- *Tbx2* and *Tbx3* promotes cell fate maturation of the OV
- *Tbx2* and *Tbx3* double conditional knockout OVs accumulate otic progenitor cells

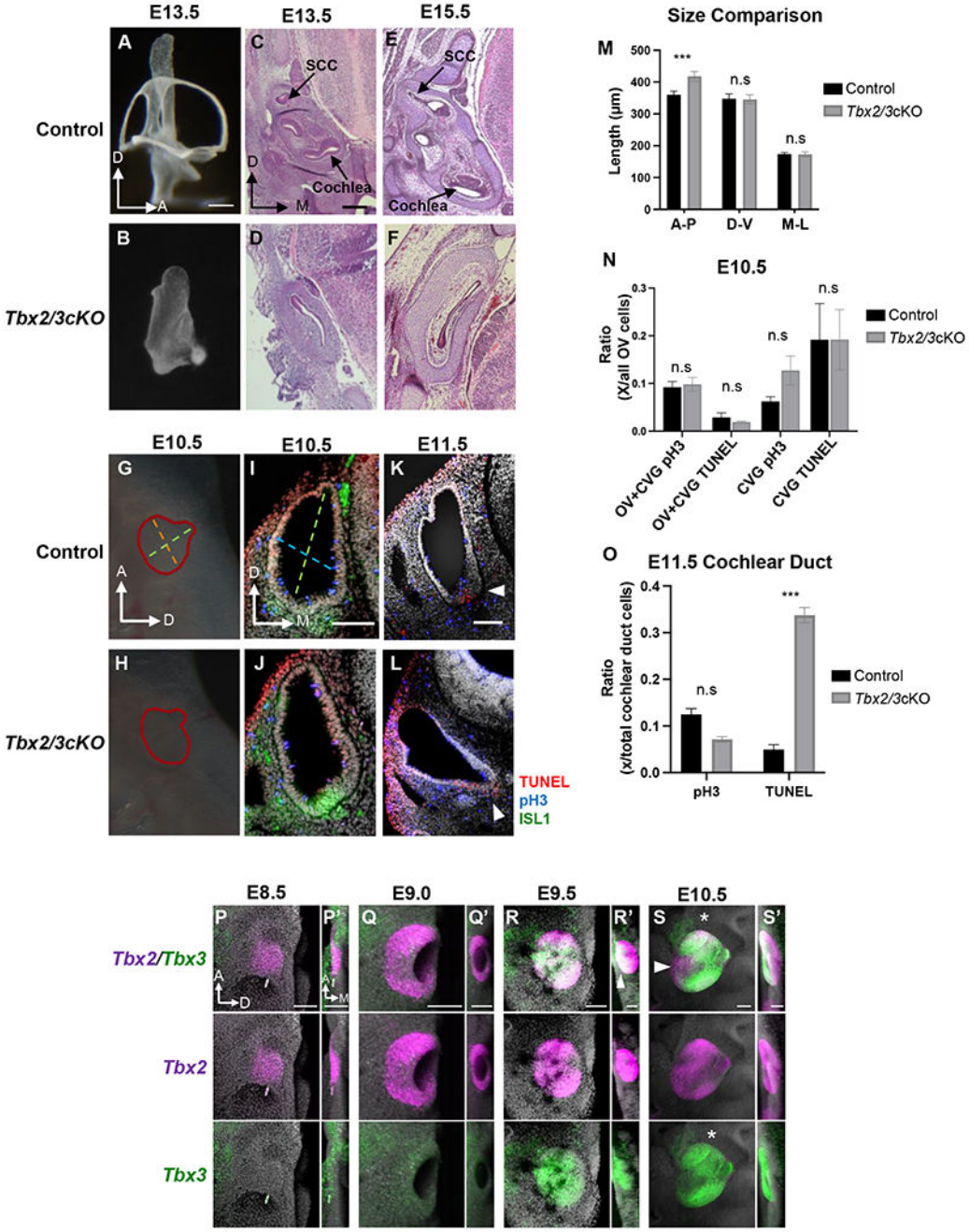

Fig. 1. *Tbx2/3*cKO embryos have failed inner ear morphogenesis; *Tbx2* and *Tbx3* are co-expressed in the OV.

(A-B) Paint filling and H&E staining **(C-D)** of E13.5 (N=6) and **(E-F)** H&E staining of E15.5, (N=4) control and *Tbx2/3*cKO embryos as indicated. **(G)** Anteroposterior axis (A-P; orange line) and dorsoventral axis (D-V; green line) was used for measurements of the OV at E10.5. Orientation of the OV with respect to the embryo is shown (A-anterior; D-dorsal). There was no significant difference in the mediolateral axis in *Tbx2/3*cKO (N=9 OVs) versus controls (N=6 OVs). **(H)** Elongation of the A-P axis of the OV in

*Tbx2/3*cKO embryos was observed. No significant difference was found in the D-V axis. **(I)** Measurements of the OV (mediolateral axis, blue line; dorsoventral axis, green line) at E10.5. Orientation of the OV is shown (D-dorsal, M-medial). **(I-L)** Immunofluorescence of sections using anti-pH3 (blue) and TUNEL (red) assays of control and *Tbx2/3*cKO embryos at E10.5 **(I-J)** and at E11.5 **(K, L)**; DAPI in gray, anti-ISL1 in green. **(M)** Size comparison of OVs in *Tbx2/3*cKO embryos (N=14 OVs) and controls (N=18 OVs) shows significant expansion of the anterior-posterior, A-P axis in *Tbx2/3*cKO embryos (three stars; P-value=4.667e-05). Dorsal-ventral (D-V) and medial-lateral (M-L) is indicated. **(N)** Proliferation and apoptosis rates of OV and CVG, marked by anti-ISL1 in controls (N=6 OVs) and *Tbx2/3*cKO (N=6 OVs) OVs at E10.5. **(K, L)** Gross increased apoptosis in the cochlear duct was observed in the OVs of *Tbx2/3*cKO embryos at E11.5 (control N=5 OVs, *Tbx2/3*cKO N=6 OVs). **(O)** Significant increase in apoptosis was found in the cochlear ducts of *Tbx2/3*cKO embryos as quantified by TUNEL assays (P-value =1.79e-07). No significant difference in proliferation was detected in the cochlear duct at E11.5. **(P-S')** wmRNAscope experiments show the spatiotemporal expression pattern of *Tbx2* (magenta) and *Tbx3* (green) from E8.5 through E10.5. **(P, P' and R, R')** *Tbx2* expression was initiated at E8.5 in the otic placode and was expressed throughout the OV at E9.5. **(Q, Q' and R, R')** *Tbx3* expression was initiated at E9.0 and E9.5 in the lateral otic cup (**R'**, arrowhead). **(S)** Expression of *Tbx2/3* is shared in most but not all domains of the OV. Note unique expression of *Tbx2* was in the ventral (**S**, arrowhead) and medial domains of the OV, and *Tbx3* had unique expression in the CVG (**S**, asterisk). N=4 for each timepoint. Orientation of the OV with respect to the embryo is shown (A-anterior; D-dorsal). A-B scale bar: 100μm; C-F scale bar: 200μm; I-L scale bar: 200μm; P-S' scale bar: 100μm.

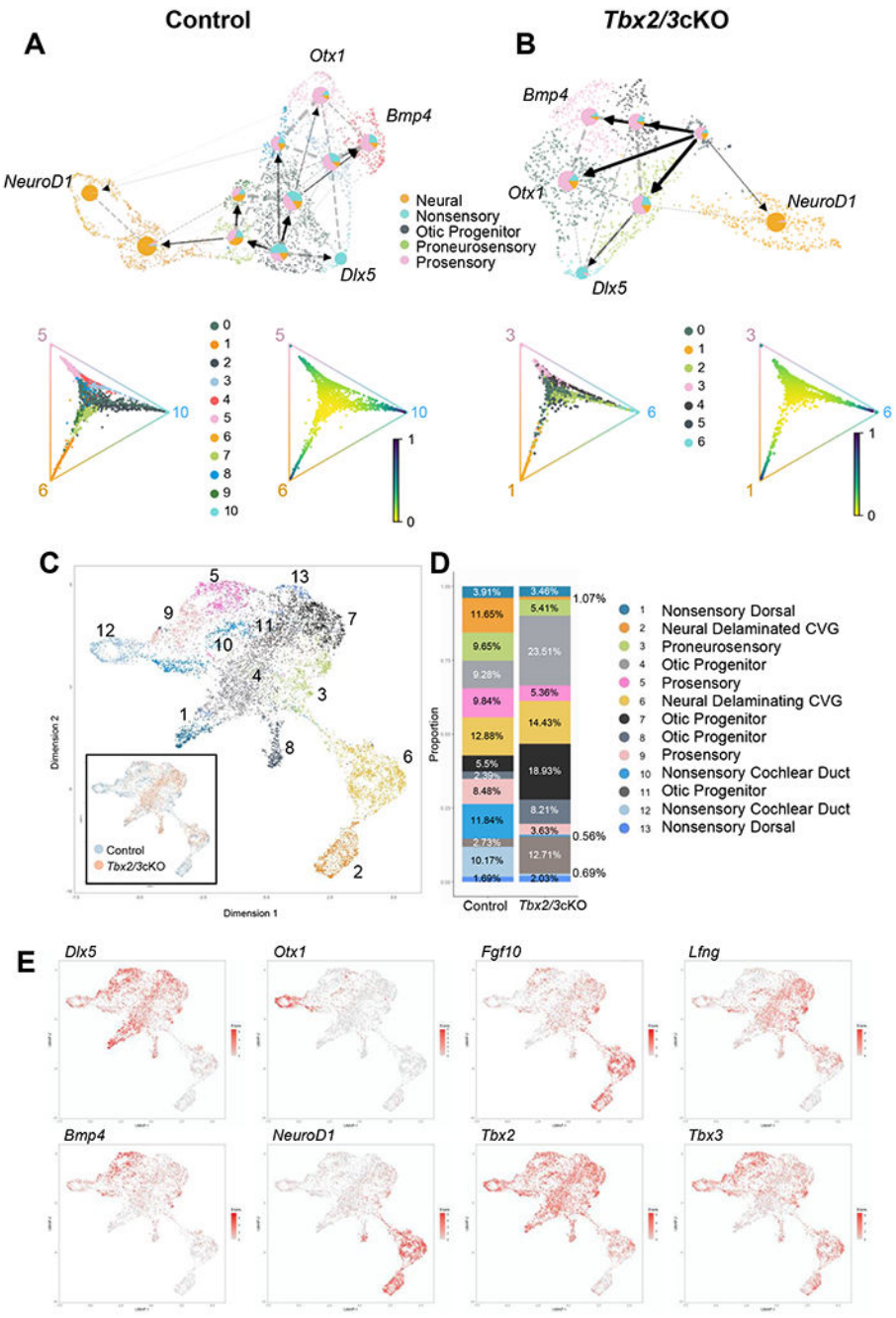

Fig. 2. Loss of Tbx2/3 causes accumulation of otic progenitor cells and delayed differentiation.

(A-B) Directed PAGA plots of RNAvelocity and circular projections of fate probabilities for prosensory, nonsensory, and neural terminal developmental states. Otic progenitor cells that are expanded in *Tbx2/3*cKO embryos, are indicated (gray in UMAP). **(C)** UMAP of integrated control and *Tbx2/3*cKO data distribution and clusters. **(D)** Proportion of clusters between control and *Tbx2/3*cKO embryos. Proportions of clusters per genotype. P-values were calculated for each cluster using the two proportion Z test at a confidence interval of 95%: Clusters 2 to 5 and 7 to 12, had a P-value < 0.00001, Cluster 1, P-value = 0.25848,

Cluster 6, P-value =0.03078, Cluster 13, P-value = 0.2246. **(E)** Markers used to identify clusters of the OV. *Dlx5* for dorsal nonsensory, *Otx1* for ventral nonsensory, *Fgf10* and *Lfng* for proneurosensory, *Bmp4* for prosensory, and *NeuroD1* for neural clusters. The expression of *Tbx2/3* is also shown.

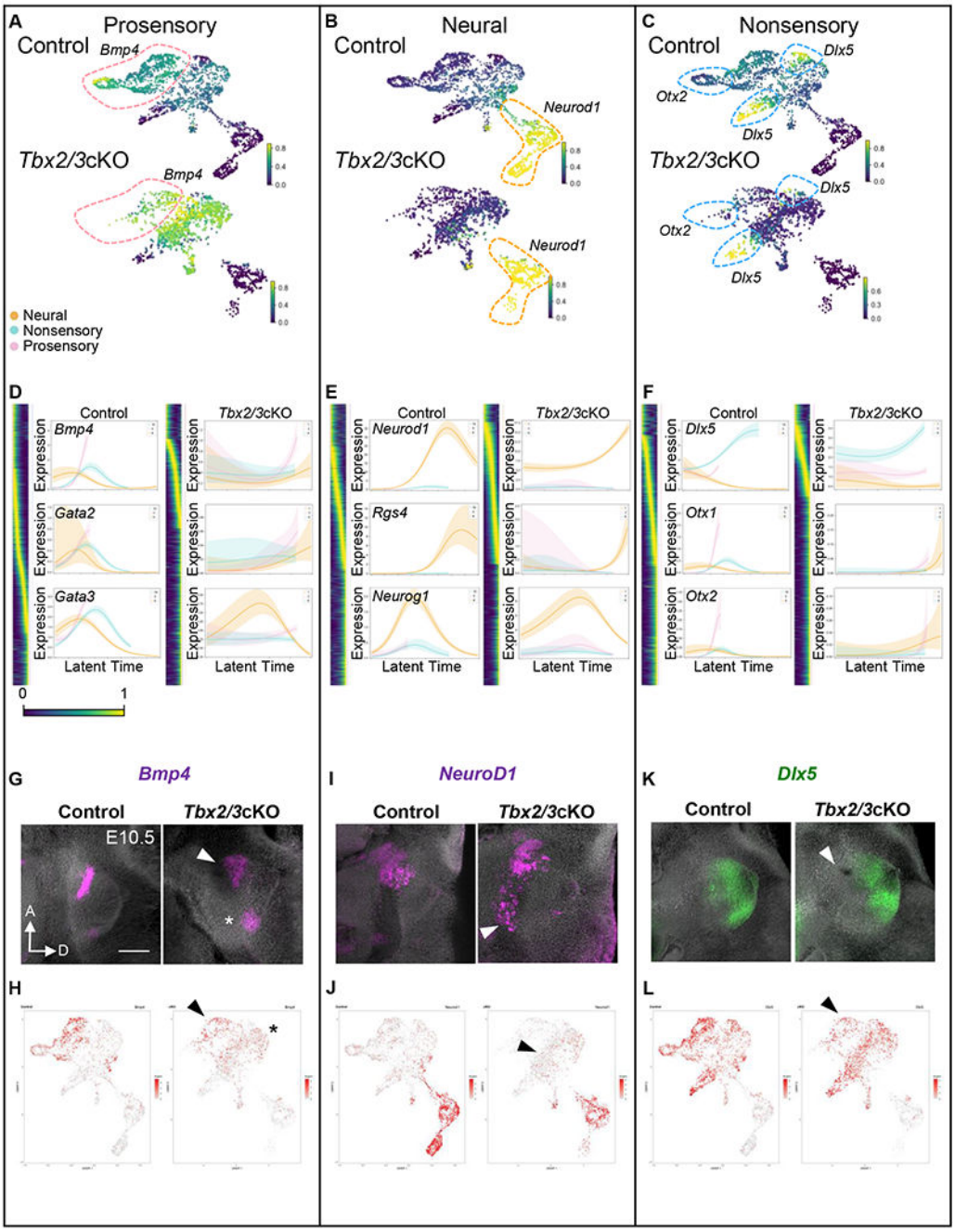

Fig. 3. Delayed differentiation of sensory and nonsensory lineages in *Tbx2/3*cKO OVs.

(A–C) Absorption probabilities representing the progression of each cell to more differentiated terminal states for control and *Tbx2/3*cKO embryos (purple to yellow, low to high). **(D–F)** Miniaturized heat maps of lineage genes that were also identified as DEGs between control and *Tbx2/3*cKO embryos for prosensory, neural and nonsensory cells as indicated. Example of representative lineage markers for each terminal state were shown in more detail on expression vs developmental latent time, referred to as latent time for each cell type. **(G-H)** *Bmp4* (control, N = 7; *Tbx2/3*cKO, N = 5) expression at

E10.5 was ventrally expanded in *Tbx2/3*cKO embryos (arrowhead, G). Lateral expansion of the posterior prosensory expression domain of *Bmp4* is indicated (asterisk, G). *Bmp4* was slightly decreased in the prosensory domain (arrowhead, H) and increased in otic progenitors (asterisk, H) in the UMAP plots. **(I-J)** Expression of *NeuroD1* (control, N = 6; *Tbx2/3*cKO, N = 4) in *Tbx2/3*cKO OVs was posteriorly expanded (arrowhead, I) and expanded in the otic progneitors (arrowhead, J). **(K-L)** *Dlx5* (control, N = 4; *Tbx2/3*cKO, N = 4) expression regressed dorsally; loss of Dlx5 expression in the prosensory domain is indicated (arrowhead). Scale bar: 200 μm.

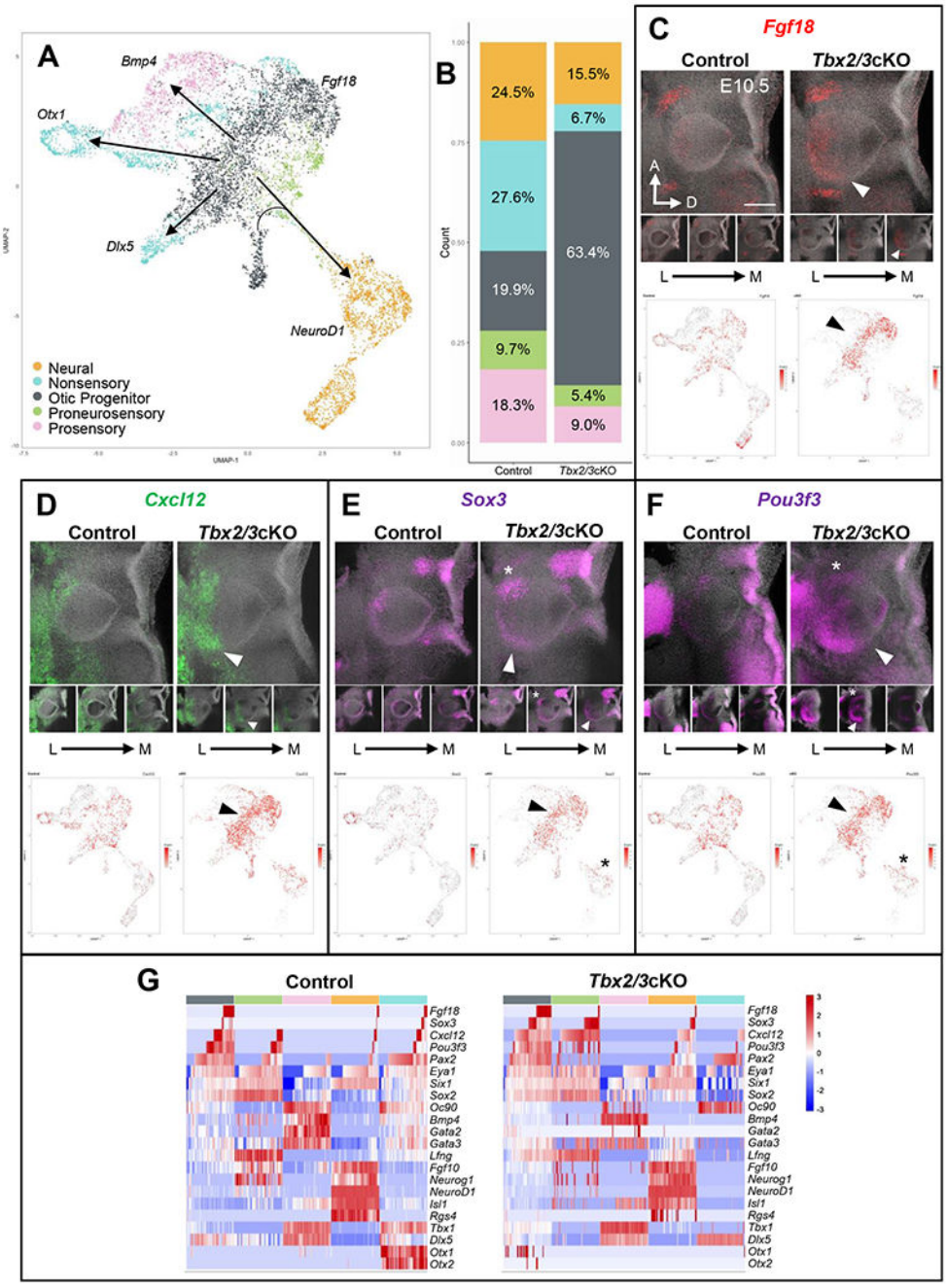

Fig. 4. Dysregulation of gene expression in otic progenitors in *Tbx2/3*cKO embryos.

(A) Summary of compiled cell lineage types identified in the integrated scRNA-seq data from Fig. 2A–B and Fig. S8A–B. **(B)** Distribution of cell lineage types in control vs *Tbx2/3*cKO embryos with colors indicated in **A**. Two proportion Z test at a confidence interval of 95% indicated significant difference for the populations of cell types in control vs *Tbx2/3*cKO with a P-value < 0.00001. **(C)** *Fgf18* expression was increased in the OVs in *Tbx2/3*cKO embryos as observed by wmRNAscope (arrowhead). Insert shows three digital sections of the whole mount images, from the lateral to medial regions of the OV (L-M,

arrow). Expression in the otic progenitors was identified in the UMAP of *Tbx2/3*cKO OVs (arrowhead). **(D)** *Cxcl12* expression was expanded to the posterior OV (wmRNAscope; digital images are shown in insert) and in the otic progenitors (UMAP), arrowhead. **(E)** *Sox3* expression was increased in the CVG (three digital images are shown), asterisk, and in the otic progenitors in the posterior OV (UMAPs) of *Tbx2/3*cKO mutant embryos. **(F)** *Pou3f3* expression is expanded dorsally from its original ventral expression, including in the CVG, asterisk, and the otic progenitors, arrowhead. **(G)** Heat map of co-expression of representative marker genes for the otic progenitor, proneurosensory, prosensory, neural and nonsensory cell types, indicated by color above the map. Expression levels are indicated in the bar on the right with strongest expression in red and weakest in blue.

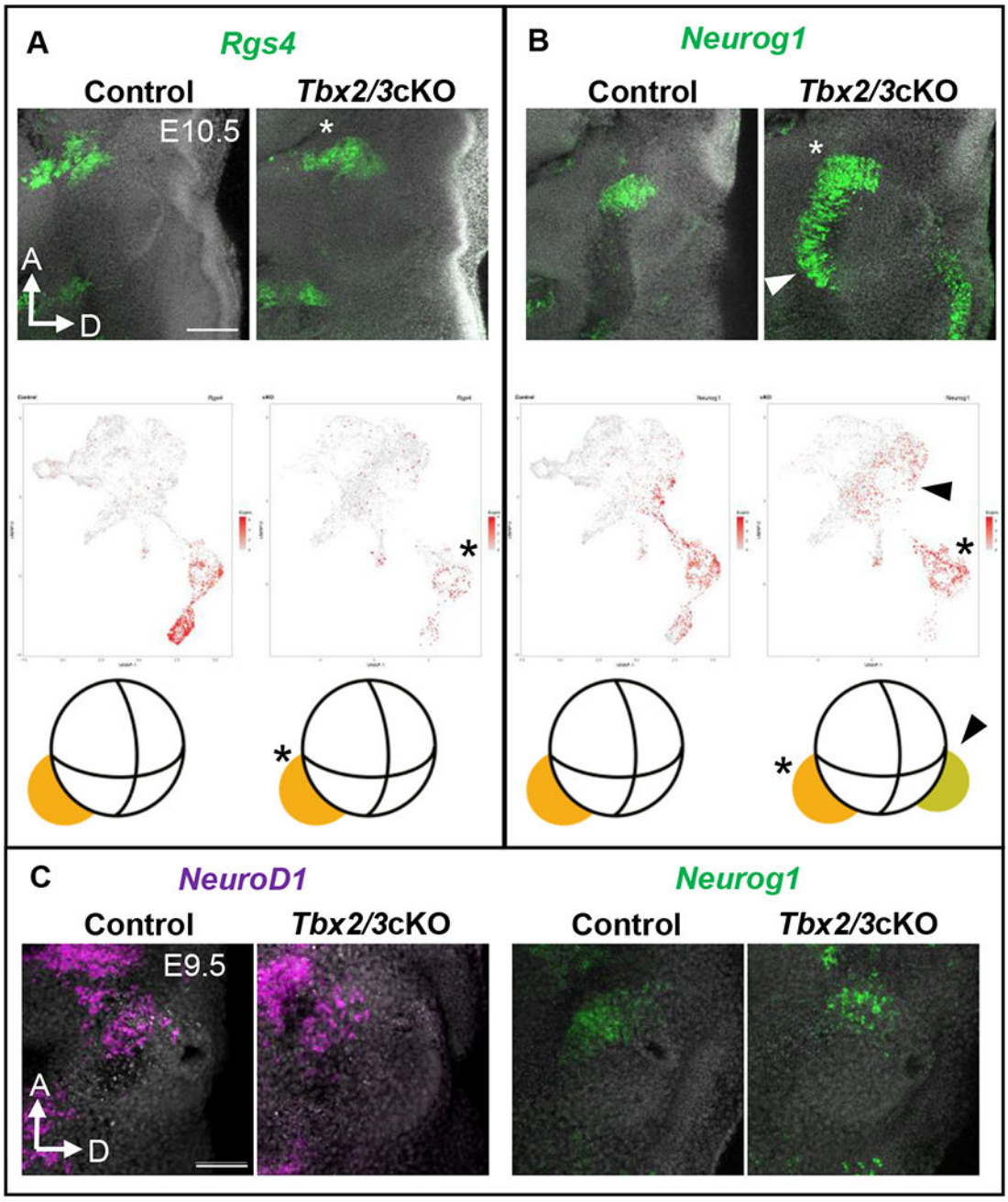

Fig. 5. Delayed differentiation of neural cells in ectopic posterior domain of the OV.

(A) *Rgs4* (Control, N=4; *Tbx2/3*cKO, N=4) expression in the CVG in both control and *Tbx2/3*cKO embryos is similar, asterisk indicates delaminated CVG cells in the wmRNAscope and UMAP images. In the wmRNAscope image, there was some expression posterior to the OV but this is cranial nerve IX (glossopharyngeal nerve). The CVG is indicated in the cartoon in orange. **(B)** Expression of *Neurog1* (Control, N=9; *Tbx2/3*cKO, N=10) in the anterior CVG region was similar between control and *Tbx2/3*cKO, asterisk in wmRNAscope, cartoon (orange) and UMAP images. Expression was expanded in the

ventral and posterior OV region as visualized by wmRNAscope (arrowhead). Expression was detected in the otic progenitor region of the UMAPs, which may correspond to the ventral and posterior OV region in the embryo. Cartoon is shown indicating comparable position as by wmRNAscope with altered color indicating that these cells are in a different developmental state (lime green). **(C)** *NeuroD1* (Control, N=4; *Tbx2/3*cKO, N=4) and *Neurog1* (Control, N=4; *Tbx2/3*cKO, N=4) were expressed only in the anterior ventral OV region in control and *Tbx2/3*cKO embryos at E9.5.

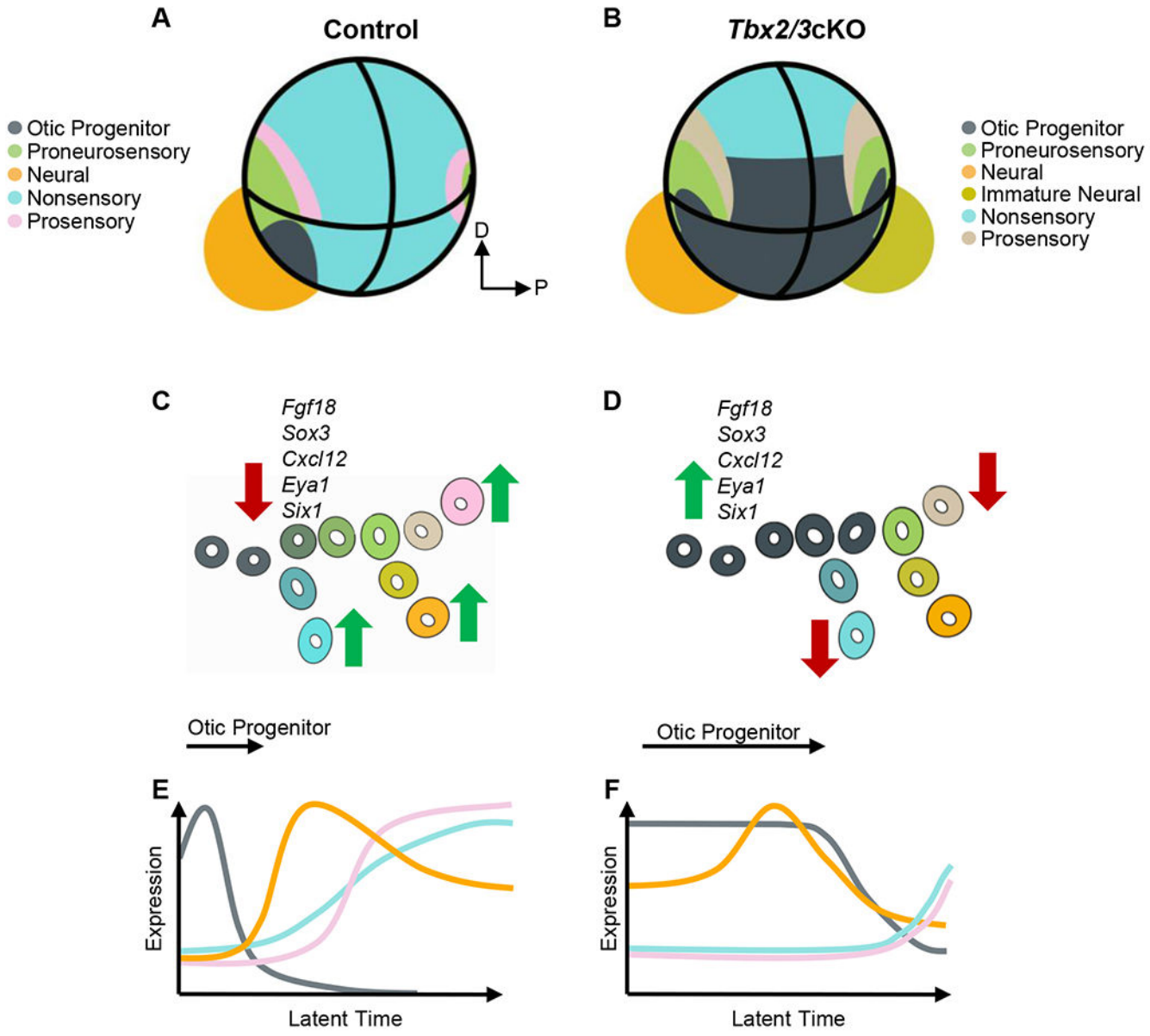

Fig. 6. Model of inner ear development and *Tbx2/3* function in restricting cell fate progression of otic progenitors.

(A-B) Cartoon representing normal development of major cell types in the inner ear in control and *Tbx2/3*cKO OVs at E10.5. Colors indicate different cell types and states (muted colors of prosensory and neural states in B). Axes are indicated (D, dorsal; P, posterior). **(C-D)** Normal differentiation of the otic progenitors (colored cartoons of cells, nuclei are white) into the three terminal states, nonsensory, neural, and sensory. Green arrows indicate increased expression in pseudotime, while red arrows indicate decreased expression. There was continued expression of otic progenitor genes and loss of cells of terminal fates in *Tbx2/3*cKO OVs as determined by pseudotime analysis. Arrow below cartoon indicates relative increase of otic progenitors in mutant embryos. **(E-F)** Summarized expression vs latent time graph representing marker genes (otic progenitor markers, gray; neural markers,

orange; prosensory markers, pink; nonsensory markers, blue) of otic progenitors and each terminal lineage in control and *Tbx2/3*cKO OVs.